Am J Cancer Res 2022;12(11):5160-5182
www.ajcr.us /ISSN:2156-6976/ajcr0146047

Original Article

Development and clinical validation of a necroptosis-related gene signature for prediction of prognosis and tumor immunity in lung adenocarcinoma

Kai Lei[1,2*], Binghua Tan[1,2*], Ruihao Liang[1,2*], Yingcheng Lyu[1,2], Kexi Wang[1,2], Wenjian Wang[1,2], Kefeng Wang[1,2], Xueting Hu[1,2], Duoguang Wu[1,2], Huayue Lin[1,3], Minghui Wang[1,2]

[1]Guangdong Provincial Key Laboratory of Malignant Tumor Epigenetics and Gene Regulation, Sun Yat-sen Memorial Hospital, Sun Yat-sen University, Guangzhou, Guangdong, China; [2]Department of Thoracic Surgery, Sun Yat-sen Memorial Hospital, Sun Yat-sen University, Guangzhou, Guangdong, China; [3]Breast Tumor Center, Sun Yat-sen Memorial Hospital, Sun Yat-sen University, Guangzhou, Guangdong, China. [*]Equal contributors and co-first authors.

Received August 20, 2022; Accepted November 8, 2022; Epub November 15, 2022; Published November 30, 2022

Abstract: Necroptosis is a new programmed formation of necrotizing cell death, which plays important role in tumor biological regulation, including tumorigenesis and immunity. In this study, we aimed to establish and validate a prediction model based on necroptosis-related genes (NRGs) for lung adenocarcinoma (LUAD) prognosis and tumor immunity. The training set consisted of samples from The Cancer Genome Atlas (TCGA) dataset (n = 334), and the validation sets consisted of samples from the Gene Expression Omnibus (GEO) (n = 439) and clinical (n = 20) datasets. Gene Oncology (GO) and Kyoto Encyclopedia of Genes and Genomes (KEGG) pathway analysis showed that 28 necroptosis-related differentially expressed genes (DEGs) were enriched in cell death and immune regulation. RT-qPCR and western blot results showed the low expression of necroptosis markers in LUAD cells. A prognostic gene signature based on 6 NRGs (*PYGB*, *IL1A*, *IFNAR2*, *BIRC3*, *H2AFY2*, and *H2AFX*) was constructed and the risk score was calculated. Multivariate Cox regression analysis showed that the risk score was an independent risk factor [hazard ratio (HR) = 1.220, 95% confidence interval (CI): 1.154-1.290, P<0.001]. In the TCGA cohort, a high-risk score was associated with poor prognosis, weak immune infiltration, and low expression at immune checkpoints, which was validated in the GEO and clinical cohorts. Our findings showed that the patients in the low-risk group had a better progression-free survival (PFS) [not reached vs. 8.5 months, HR = 0.18, 95% CI: 0.04-0.72, P<0.001] than those in the high-risk score group. Immunotherapy tolerance was found to be correlated with the high-risk score, and the risk score combined with PD-L1 (AUC = 0.808, 95% CI: 0.613-1.000) could better predict the immunotherapy response of LUAD. A nomogram was shown to have a strong ability to predict the individual survival rate of patients with LUAD in the TCGA and GSE68465 cohorts. We constructed and validated a potential prognostic signature consisting of 6 NRGs to predict the prognosis and tumor immunity of LUAD, which may be helpful to guide the individualized immunotherapy of LUAD.

Keywords: Necroptosis, lung adenocarcinoma, prognosis, tumor microenvironment, immunotherapy

Introduction

Lung cancer has always been known as a malignant tumor for its high incidence and unfavorable prognosis [1, 2]. As emphasized in the current report of global cancer statistics [3], lung cancer ranked second and first in the global cancer incidence and death spectrum in 2020, accounting for 11.4% of the total number of new cancer cases and 18% of the total cancer deaths, respectively. Clinically, lung adenocarcinoma (LUAD) is one of the most common pathological types of non-small cell lung cancer (NSCLC), accounting for about 40% of all lung cancer cases [4]. Although surgery, chemotherapy, radiotherapy, and targeted therapy have made significant progress in the treatment of LUAD, the 5-year survival rate of LUAD is still less than 20% [2, 5].

The applications of immune checkpoint inhibitors (ICIs) targeting programmed cell death pro-

tein 1 (PD-1), programmed cell death 1 ligand 1 (PD-L1), and cytotoxic T lymphocyte-associated antigen 4 (CTLA4) have made revolutionary progress in the treatments of lung cancer and greatly prolonged the survival time of patients with advanced NSCLC [6]. However, only a small number of tumor patients respond to immunotherapy [7, 8]. The tumor immune microenvironment (TIME) determined by tumor-infiltrating immune cells was closely related to tumorigenesis, tumor metastasis, and tumor immune escape, and affected the sensitivity of immunotherapy and the survival of cancerous patients [9]. Due to the heterogeneity and complexity of tumors, the curative effect is variable in different populations. At present, no accurate biomarkers were available to predict immunotherapy response in cancerous patients for potential beneficiary selection. Although PD-L1 expression, tumor mutation burden (TMB) level, and immune cell infiltration in the tumor microenvironment (TME) were related to the outcome of immunotherapy [10], the performance of these indicators in LUAD was still insufficient. Therefore, the exploration of novel biomarkers for tumor prognostic and immunological characteristics is crucial for optimizing the prognosis evaluation system and individualized treatment strategy of LUAD.

Necroptosis is an important type of programmed cell death in addition to apoptosis, with morphological characteristics of necrotic cell death, such as lysosomal membrane degradation, cytoplasmic vacuolization, plasma membrane disintegration, and finally cell rupture [11]. Necroptosis is mainly regulated by RIPK1 (receptor-interacting protein kinase 1) and RIPK3 (receptor-interacting protein kinase 3), which assemble into an oligomeric complex termed the necrosome [12, 13]. MLKL (mixed lineage kinase domain-like pseudokinase) is activated by RIPK1/RIPK3 complex mediated phosphorylation signal pathway, oligomerized and transported to the cell membrane, which quickly leads to necrotizing plasma membrane permeability, destroying cell integrity and necroptosis [14]. Necroptosis is a new form of programmed cell death that is caspase-independent [15] and plays a dual role in tumorigenesis, metastasis, tumor immunity, and prognosis [14, 16]. Necroptosis leads to a chronic inflammatory response by recruiting a large number of immune-inflammatory cells, thus promoting tumor metastasis and immunosuppression [17, 18]. The expression of RIPK1 and RIPK3 was decreased in breast cancer [19] and malignant melanoma patients [20]. Park et al. [21] found that increased expression of RIPK1 was associated with poor prognosis in glioblastoma. Feng et al. [22] found that low expression of RIPK3 was associated with malignant progression and poor prognosis in colorectal cancer.

Nevertheless, the role of necroptosis in the development of lung cancer remains controversial. Some studies have shown that RIP1 [23] and RIP3 [24] are obviously overexpressed in human NSCLC, which promotes tumor progression and poor prognosis. Other studies have shown that the expression of key necroptosis-regulating genes such as *RIPK1*, *RIPK3*, and *MLKL*, is down-regulated in NSCLC, which is positively related to tumor recurrence, poor prognosis [25], and chemotherapy resistance [26]. Therefore, it is necessary to further explore the relationship between necroptosis and the progression and prognosis of LUAD. Moreover, autophagy [27], ferroptosis [28], and pyroptosis [29] related gene signatures have been reported to play an important role in predicting the prognosis and tumor immunological characteristics of LUAD. However, as a way of programmed cell death, necroptosis has not been well investigated.

The aim of this study was to generate and verify a necroptosis-related gene (NRG) signature, which could predict the prognosis and tumor immunological characteristics of LUAD and guide the individualized treatment of LUAD. Firstly, we studied the characteristics of necroptosis-related differentially expressed genes (DEGs) in LUAD by enrichment analysis. Then, the NRG signature for assessing the prognosis, tumor immune infiltration, and immunotherapy sensitivity of LUAD was constructed in the training set, and the effectiveness of the model was verified in the validation sets. Finally, a nomogram for predicting the individual survival probability of LUAD was established and verified.

Materials and methods

Acquisition of the NRGs list and mRNA expression profiles

The mRNA expression profiles (FPKM) and clinicopathological features from the TCGA TARGET GTEx dataset were downloaded through the

Table 1. The clinical characteristics of LUAD patients in the training and validation cohorts

	TCGA cohort (Training set) (n = 334)	GSE68465 cohort (Validation set) (n = 439)	statistical value	*p*-value
Age			1.397	0.237
<65	147 (44%)	212 (48.3%)		
≥65	187 (56%)	227 (51.7%)		
Gender			0.024	0.878
Male	170 (50.9%)	221 (50.3%)		
Female	164 (49.1%)	218 (49.7%)		
pT stage			4.124	0.042*
T1-T2	289 (86.5%)	400 (91.1%)		
T3-T4	45 (13.4%)	39 (8.9%)		
pN stage			2.059	0.151
N0	211 (63.2%)	299 (68.1%)		
N1-N3	123 (36.8%)	140 (31.9%)		
Survival state			12.475	<0.001***
Live	198 (59.3%)	204 (46.5%)		
Die	136 (40.7%)	235 (53.5%)		

*P<0.05, ***P<0.001.

University of California Santa Cruz Xena platform (UCSC Xena; https://xena.ucsc.edu/). Five hundred and thirteen LUAD cases were obtained from The Cancer Genome Atlas database (TCGA; https://cancergenome.nih.gov/). Among them, 334 cases with mRNA expression data, survival information, and clinical characteristics were used for survival analysis. Two hundred and eighty-seven normal lung samples were obtained from the Genome Tissue Expression database (GTEx; https://commonfund.nih.gov/GTEx/). A total of 159 genes related to the necroptosis pathway were obtained by searching the ID of the human necroptosis pathway "hsa04217" on the Kyoto Encyclopedia of Genes and Genomes database (KEGG; https://www.genome.jp/dbget-bin/www_bget?pathway:hsa04217), and 131 of them were expressed in the TCGA-LUAD dataset. The inclusion criteria of LUAD cases used for subsequent prognostic analysis and model development were as follows: 1) detailed transcriptomic data; 2) detailed clinicopathological data and prognostic information. Therefore, the TCGA-LUAD dataset including 334 LUAD samples and 131 NRGs was used as the training set. The GSE68465 dataset including 439 LUAD cases was downloaded from the Gene Expression Omnibus database (GEO; https://www.ncbi.nlm.nih.gov/geo/) and used as the validation set. The basic clinical features of the training set and validation set were listed in **Table 1**.

Identification and enrichment analysis of necroptosis-related DEGs

The principal component analysis (PCA) was performed to detect batch effects from the TCGA-LUAD and GTEx datasets. The R package "limma" was used to find necroptosis-related DEGs between LUAD and normal samples in the TCGA TARGET GTEx cohort. The cutoff criteria were adjusted *p*-value <0.05 and $|\log_2 FC| > 1$. The differential expression of NRGs was visualized by a heatmap, a volcano map, and a box plot. The R package "maftools" was used to analyze the NRG mutation landscape of 399 LUAD patients from the TCGA-LUAD dataset. The R package "clusterprofiler" was used to carry out Gene Ontology (GO) and Kyoto Encyclopedia of Genes and Genomes (KEGG) analysis on the necroptosis-related DEGs. The String database (https://string-db.org/) was used to construct the protein-protein interaction (PPI) networks of the necroptosis-related EGs, and the Cytoscape software was used to visualize the interactions of the PPI networks. The correlation heatmap of DEGs was carried out using the R package "corrplot".

Construction and validation of the NRG prognostic signature

Univariate Cox regression analysis was performed to identify the NRGs with prognostic significance in the TCGA-LUAD dataset. To mini-

mize the risk of overfitting, the generated genes were screened by LASSO regression analysis using the R package "glmnet" [30]. Independent prognostic genes related to necroptosis in LUAD were obtained by multivariate Cox regression analysis, and the NRG prognostic signature was established. We used the multivariate Cox risk regression coefficient of each NRG in the final prognosis model and the expression of each gene to calculate the risk score. The calculation formula was as follows:

$$\text{risk score} = \sum_{i=1}^{n} \text{expression}(i) * \text{coefficient}(i)$$

The TCGA-LUAD dataset was divided into two risk-score groups according to the median risk score as the cut-off value. Univariate and multivariate Cox regression analysis was used to study the prognostic value of the risk score for LUAD, and the Kaplan-Meier curve was used to assess the effect of the risk score on overall survival (OS). The receiver-operating characteristic (ROC) curve was used to compare the accuracy of risk score and clinical data in predicting the prognosis of LUAD.

Tumor immune cell infiltration analysis

Gene Set Enrichment Analysis (GSEA) was performed between the two risk score subgroups. ESTIMATE is a tool using expression data to estimate the stromal and immune cells in malignant tumor tissues. The TME scores for each patient were quantified by the R package "estimate", which includes ESTIMATEScore, ImmuneScore, StromalScore, and TumorPurity [31]. CIBERSORT algorithm was used to calculate the proportion of 22 immune cells infiltrating based on the LM22 signature. The single-sample gene set enrichment analysis (ssGSEA) from the R package GSVA [32] was employed to assess the expression levels of 28 immune cells.

The clinical validation of the 6 NRG signature

Real-time quantitative polymerase chain reaction (RT-qPCR) was used to detect the mRNA expression levels of 6 NRGs in clinical samples, and the same method as the training set was used to calculate the risk score and construct the prognostic model. The clinical samples were divided into two groups according to the median risk score, and the protein expression levels of immunomodulatory targets in the two groups were evaluated by Immunohistochemistry (IHC).

Construction and validation of the predictive nomogram

The R packages "rms" and "survival" were used to construct the nomogram, and the prognosis was predicted by combining the risk score and other clinicopathological features of LUAD patients. The time-dependent ROC curve and calibration curve of the clinical and GSE68465 cohorts were drawn to evaluate and verify the accuracy of the prognostic model.

Collection of the LUAD samples

The tumor tissues, clinicopathological data, and immunotherapy efficacy of LUAD patients who underwent surgery at Sun Yat-sen Memorial Hospital of Sun Yat-sen University from 2018 to 2020 were collected with informed consent and approval of the Medical Ethics Committee of Sun Yat-sen Memorial Hospital of Sun Yat-sen University. Inclusion criteria were as follows: 1) patients received surgical treatment and postoperative pathological diagnosis of LUAD; 2) patients received immunotherapy after tumor recurrence; 3) patients had complete clinical data, including basic clinical features, tumor pathological stage, survival prognosis, and immunotherapy response evaluation. A total of 20 LUAD patients were included in this study, including 7 males (35%) and 13 females (65%), with a median age of 68 ([59.75, 70.75]). The criteria for evaluating the efficacy of immunotherapy in LUAD patients refer to RECIST (response evaluation criteria in solid tumors) [33]. The interval between the two follow-up responses was 6-12 weeks. The clinical efficacy classification of immunotherapy included complete response (CR), partial remission (PR), stable disease (SD), and progressive disease (PD). The LUAD patients with immunotherapy effects of CR and PR were defined as the immunotherapy-response group, while those with immunotherapy effects of SD and PD were defined as the immunotherapy-resistance group. The primary endpoints were progression-free survival (PFS) and objective response rate (ORR). The risk score for each sample was calculated using the same method as before. According to the median risk score, the clinical samples were divided into the high-risk score group and the low-risk score group. The clinico-

Table 2. Comparison of general data between two immunotherapy sensitivity subgroups in the clinical cohort

	Immunotherapy resistance (SD + PD, n = 11)	Immunotherapy response (CR + PR, n = 9)	statistical value	*p*-value
age	68 ([65, 76])	68 ([54, 70])	-1.219	0.239
gender			0.02a	1.000
Male	4 (36.4%)	3 (33.3%)		
Female	7 (63.6%)	6 (66.7%)		
pT stage			0.303a	0.67
T1-T2	6 (54.5%)	6 (66.7%)		
T3-T4	5 (45.5%)	3 (33.3%)		
pN stage			5.051a	0.07
N0	3 (27.3%)	7 (77.8%)		
N1-N3	8 (72.7%)	2 (22.2%)		
pTNM stage			8.811a	0.005**
I-II	4 (36.4%)	9 (100%)		
III-IV	7 (63.6%)	0 (0)		
riskScore	1.66 (5.66)	1.11 (1.15)	-2.089b	0.038*

aFisher exact probability test, bMann-Whitney U test, *P<0.05, **P<0.01.

pathological data and the efficacy of immunotherapy were summarized in **Table 2**.

Cell culture

Two human LUAD cell lines (A549 and PC9) and one human normal lung epithelial cell line (BEAS-2B) were obtained from the Shanghai Institutes for Biological Science, China. All cells were cultured in the 1640 (Gibco, Carlsbad, CA, USA) medium with 10% fetal bovine serum (Gibco) and 100 U/mL penicillin and streptomycins (HyClone, Logan, UT, USA) at 37°C in a humidified environment containing 5% CO_2.

Western blot (WB) analysis

Human normal lung epithelial cells (BEAS-2B) and human LUAD cells (A549 and PC9) were lysed with RIPA buffer (CWBIO, Beijing, China) containing 1% phosphatase and protease inhibitor and protein was extracted. The protein was separated by sodium dodecyl sulfate-polyacrylamide gel electrophoresis (SDS-PAGE) and transferred to the PVDF membrane. The membrane was sealed with 5% bovine serum albumin solution at room temperature for 1 h, and the closed membrane was incubated with primary antibodies specific for RIPK1 (diluted 1:1000, CST, USA), RIPK3 (diluted 2000, Proteintech, Wuhan, China), MLKL (diluted 1:1000, CST, Beverly, MA, USA), TLR4 (diluted 1:1000, ABclonal, Wuhan, China), and GAPDH (diluted 1:10000, Immunoway, Newark, Delaware, USA) at 4°C overnight and then incubated with goat anti-rabbit secondary antibody for 1 h. Detection of target protein signals by using the enhanced chemiluminescence (ECL) reagent and Optimax X-ray Film Processor (Protec, Germany).

Real-time quantitative PCR

Real-time quantitative polymerase chain reaction (RT-qPCR) was used to detect the mRNA expression of 6 NRGs in the prognostic model of LUAD, and the risk score of each sample was calculated by the same method. Total RNA was extracted using TRIzol reagent (Invitrogen, Carlsbad, CA, USA). CDNA was synthesized using the PrimeScript RT Reagent Kit (TaKaRa, Otsu, Shiga, Japan). The cDNA was then analyzed by RT-qPCR using Hieff UNICON qPCR SYBR Green Master Mix (YEASEN, Shanghai, China). The expression of target transcripts was normalized to the GAPDH internal control, and relative changes in gene expression were determined using the $2^{-\Delta\Delta CT}$ method. The primers for necroptosis-related prognostic genes and immune checkpoints were shown in **Table 3**.

Immunohistochemistry (IHC)

Immunohistochemical experiments were performed according to previous methods [34]. Primary antibodies against CD3 (Immunoway),

Table 3. The primers for target genes

Primer name	Sense	Antisense
RIPK1	GGGAAGGTGTCTCTGTGTTTC	CCTCGTTGTGCTCAATGCAG
RIPK3	ATGTCGTGCGTCAAGTTATGG	CGTAGCCCCACTTCCTATGTTG
MLKL	AGGAGGCTAATGGGGAGATAG	TGGCTTGCTGTTAGAAACCTG
TLR4	AGACCTGTCCCTGAACCCTAT	CGATGGACTTCTAAACCAGCCA
PYGB	AGGTGCGGAAGAGCTTCAAC	TCGCGCTCGTAGTAGTGCT
IL-1A	TGGTAGTAGCAACCAACGGGA	ACTTTGATTGAGGGCGTCATTC
IFNAR2	TCATGGTGTATATCAGCCTCGT	AGTTGGTACAATGGAGTGGTTTT
BIRC3	TTTCCGTGGCTCTTATTCAAACT	GCACAGTGGTAGGAACTTCTCAT
H2AFY2	GCAGGTGTCATCTTTCCAGTG	CACGCTGATCCGGTACTTGA
H2AFX	GCCTCCAGTTCCCAGTG	GATGATTCGCGTCTTCTTGTTG
CD3	ACTGGCTACCCTTCTCTCG	CCGTTCCCTCTACCCATGTGA
CD8	ATGGCCTTACCAGTGACCG	AGGTTCCAGGTCCGATCCAG
FOXP3	GTGGCCCGGATGTGAGAAG	GGAGCCCTTGTCGGATGATG
PD-1	CCAGGATGGTTCTTAGACTCCC	TTTAGCACGAAGCTCTCCGAT
PD-L1	TGGCATTTGCTGAACGCATTT	TGCAGCCAGGTCTAATTGTTTT
PD-L2	ATTGCAGCTTCACCAGATAGC	AAAGTTGCATTCCAGGGTCAC
CTLA4	GCCCTGCACTCTCCTGTTTTT	GGTTGCCGCACAGACTTCA
LAG3	GCGGGGACTTCTCGCTATG	GGCTCTGAGAGATCCTGGGG
TIM3	AGACAGTGGGATCTACTGCTG	CCTGGTGGTAAGCATCCTTGG
GAPDH	AGGGGAGATTCAGTGTGGTG	GGCCTCCAAGGAGTAAGACC

CD8 (Immunoway), FOXP3 (Immunoway), PD-1 (Immunoway), and PD-L1 (Immunoway) were used. Two independent observers evaluated the immunostaining degree of the target protein. The scores of staining intensity and staining range were high positive, positive, low positive, and negative. The average optical density (AOD) of the target protein was calculated by Image J software (National Institutes of Health, Bethesda, MD, USA).

Statistical analysis

All statistical analysis were conducted by R software version 4.1.1 (R Foundation for Statistical Computing, Vienna, Austria), Statistical Product Service Solutions software (SPSS) version 26.0 (IBM Corporation, Armonk, NY, USA), and GraphPad Prism software version 7.0 (GraphPad Software, La Jolla, CA, USA). Measured data were expressed as mean standard deviation or median (quartile spacing), and the two groups comparison was analyzed by a t-test or Mann-Whitney U test. The number of cases and percentages were used to express the count data, and the chi-square test of independent samples or the Fisher exact probability method was used to compare groups. Box plot analysis was performed using the Wilcoxon signed-rank test or t-test. Survival curves were constructed by the Kaplan-Meier method using the log-rank test. $P<0.05$ is considered to be statistically significant.

Results

Differential expression and characteristics of NRGs in LUAD

The mind map of our study was shown in **Figure 1**. In the UCSC platform, the TCGA TARGET GTEx dataset contained 513 LUAD cases from the TCGA dataset and 287 normal cases from the GTEx dataset. PCA analysis found that there was consistency within the two groups (TCGA-LUAD and GTEx datasets), but differences between the groups (**Figure 2A**). A total of 159 NRGs were obtained from the KEGG website, 131 of which were expressed in the TCGA-LUAD dataset. A total of 7 upregulated genes (*PLA2G4A*, *STAT1*, *H2AFX H2AFV*, *PARP1*, *PGAM5*, and *CHMP4C*) and 21 downregulated genes (*PLA2G4F*, *TYK2*, *PLA2G4B*, *JMJD7-PLA2G4B*, *STAT6*, *PYGM*, *STAT5B*, *TNFAIP3*, *NLRP3*, *IFNGR1*, *TLR4*, *JAK2*, *IL33*, *STAT4*, *CFLAR*, *FAS*, *JAK3*, *MLKL*, *STAT5A*, *PLA2G4C*,

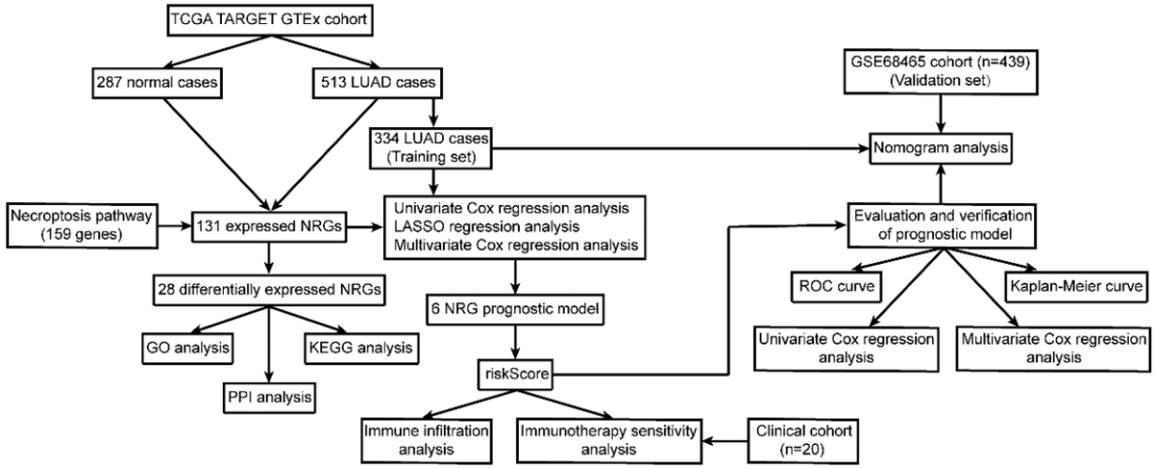

Figure 1. The workflow chart for this study.

and *CASP1*) were identified according to the criteria for adjusted *p*-value <0.05 and $|\log_2 FC| > 1$ (**Figure 2B**, **2C**). Box plots revealed the expression patterns of 28 necroptosis-related DEGs in tumor and normal tissues (**Figure 2D**). The mutational landscape revealed that 258 (64.66%) samples in the TCGA-LUAD dataset had NRG mutations, with a mutation rate of more than 3%. The two most common types of mutations were synonymous and missense mutations (Supplementary Figure 1).

Enrichment analysis of necroptosis-related DEGs and the expression of necroptosis markers

The GO functional and the KEGG pathway enrichment analysis provided a basis for further understanding the function and mechanism of 28 necroptosis-related DEGs. The top biological processes (BP) terms of the GO functional enrichment analysis were growth hormone receptor pathway via JAK-STAT and programmed necrotic cell death, the top cellular component (CC) term was inflammation complex, and the top molecular function (MF) term was hormone receptor binding (**Figure 3A**, **3B**). In the KEGG pathway enrichment analysis, the necroptosis-related DEGs were enriched in the necroptosis pathway, and the Z-scores of the enriched necroptosis pathway indicated that necroptosis was inhibited in LUAD (**Figure 3C**, **3D**). The PPI network and correlated heatmap of 28 necroptosis-related DEGs were shown in Supplementary Figure 2A, 2B. *RIPK1*, *RIPK3*, *MLKL*, and *TLR4* are considered as key molecular markers in the necroptosis pathway [35, 36]. By comparing the expression of necroptosis markers in LUAD tissues and normal tissues in the TCGA TARGET GTEx dataset, we found that the expression of necroptosis markers in LUAD was significantly lower than that in normal tissues (Supplementary Figure 3A). RT-qPCR (**Figure 3E**) and WB (**Figure 3F** and Supplementary Figure 3B) analysis showed that the expression of necroptosis markers at mRNA and protein levels were significantly lower in human LUAD cell lines (A549 and PC9) than those in human normal lung epithelial cell line (BEAS-2B).

Development of a 6 NRG prognostic signature in the TCGA-LUAD cohort

Based on the TCGA-LUAD cohort, we screened 25 genes affecting OS by using univariate Cox regression analysis (**Figure 4A**). To acquire a high-accuracy prognostic model, 16 NRGs were obtained by LASSO regression analysis (**Figure 4B**, **4C**). Finally, 6 independent prognostic genes of LUAD were obtained by multivariate Cox regression analysis (**Figure 4D**). Among them, the genes with HR>1 (*PYGB*, *IL1A*, *BIRC3*, *H2AFY2*, and *H2AFX*) were the risk genes, and the gene with HR<1 (*IFNAR2*) was the protective gene (**Table 4**). The risk score = (0.468 * expression level of PYGB) + (0.217 * expression level of BIRC3) + (0.243 * expression level of IL1A) + (0.190 * expression level of H2AFY2) + (0.264 * expression level of H2AFX) + (-0.324 * expression level of IFNAR2). According to the median risk score, LUAD cases were divided

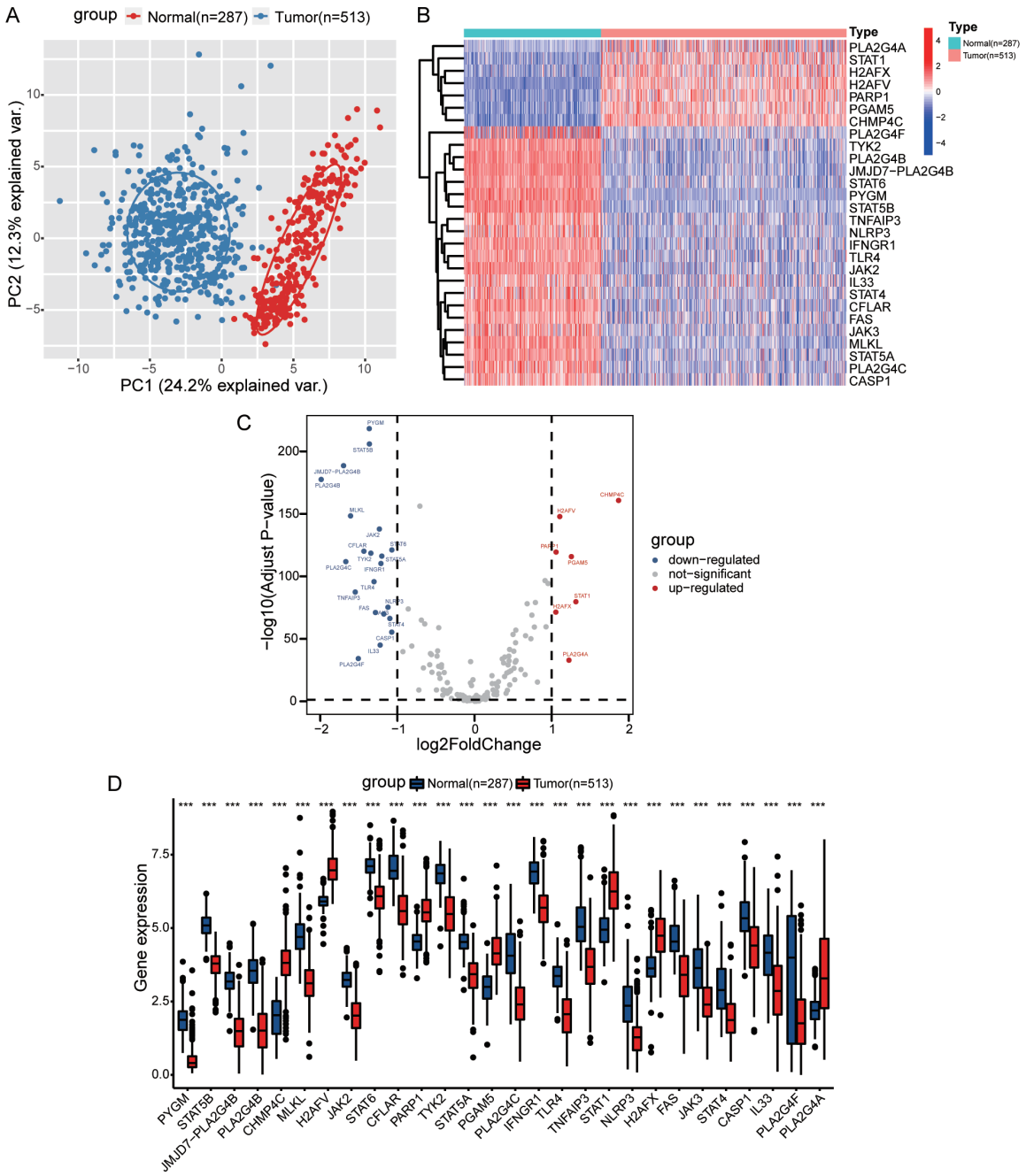

Figure 2. Differential expression of NRGs in LUAD. A. The plot of principal component analysis (PCA) between the TCGA-LUAD dataset (tumor = 513) and the GTEx dataset (normal = 287). B, C. The heatmap and volcano plot of the necroptosis-related DEGs (the filtering criteria were adjusted *p*-value <0.05 and $|\log_2 FC| > 1$). D. The expression of 28 NRGs in LUAD and normal lung tissues. The upper and lower edges of the boxes represented the upper and lower quartile margins. The horizontal lines in the boxes represented the median. LUAD: Lung Adenocarcinoma; GTEx: Genotype-Tissue Expression, ***P<0.001.

into the high-risk score group and the low-risk score group. With the increase of risk score in LUAD, the death risk increased, the OS decreased, the expression of risk genes was up-regulated, and the expression of protective genes was down-regulated (**Figure 4E**). These results were verified in the GSE68465 cohort (**Figure 4F**).

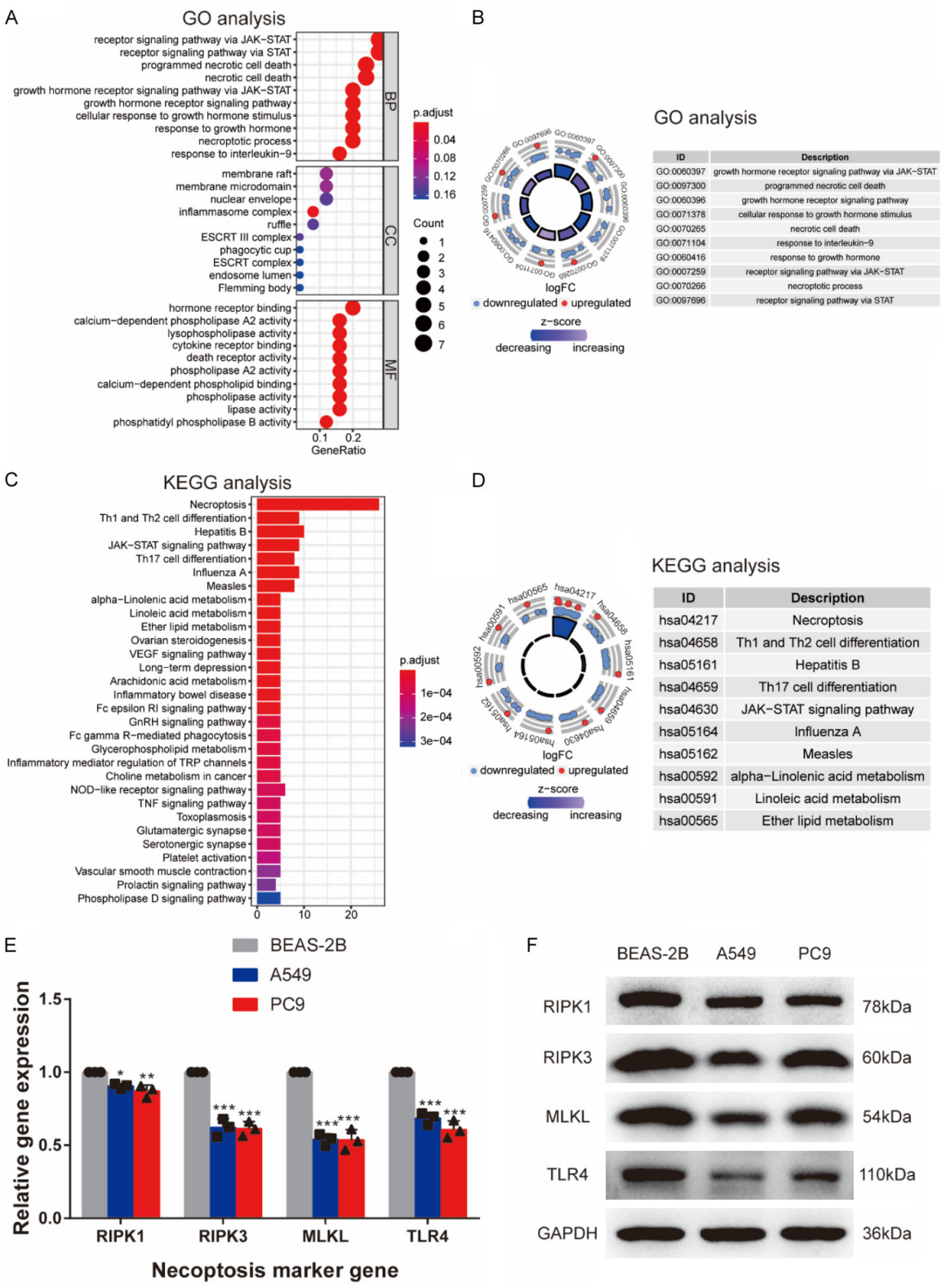

Figure 3. The functional enrichment analysis of necroptosis-related DEGs and expression levels of necroptosis markers in LUAD. A, B. GO enrichment analysis of the necroptosis-related DEGs. C, D. KEGG pathway enrichment analysis of the necroptosis-related DEGs. E. The mRNA levels of necroptosis markers in LUAD cells were detected by RT-qPCR. F. The protein levels of necroptosis markers in LUAD cells were detected by western blot. BP: Biological Process; CC: Cellular Component; MF: Molecular Function; DEGs: Differentially Expressed Genes; ns: no significance, *P<0.05, **P<0.01, ***P<0.001.

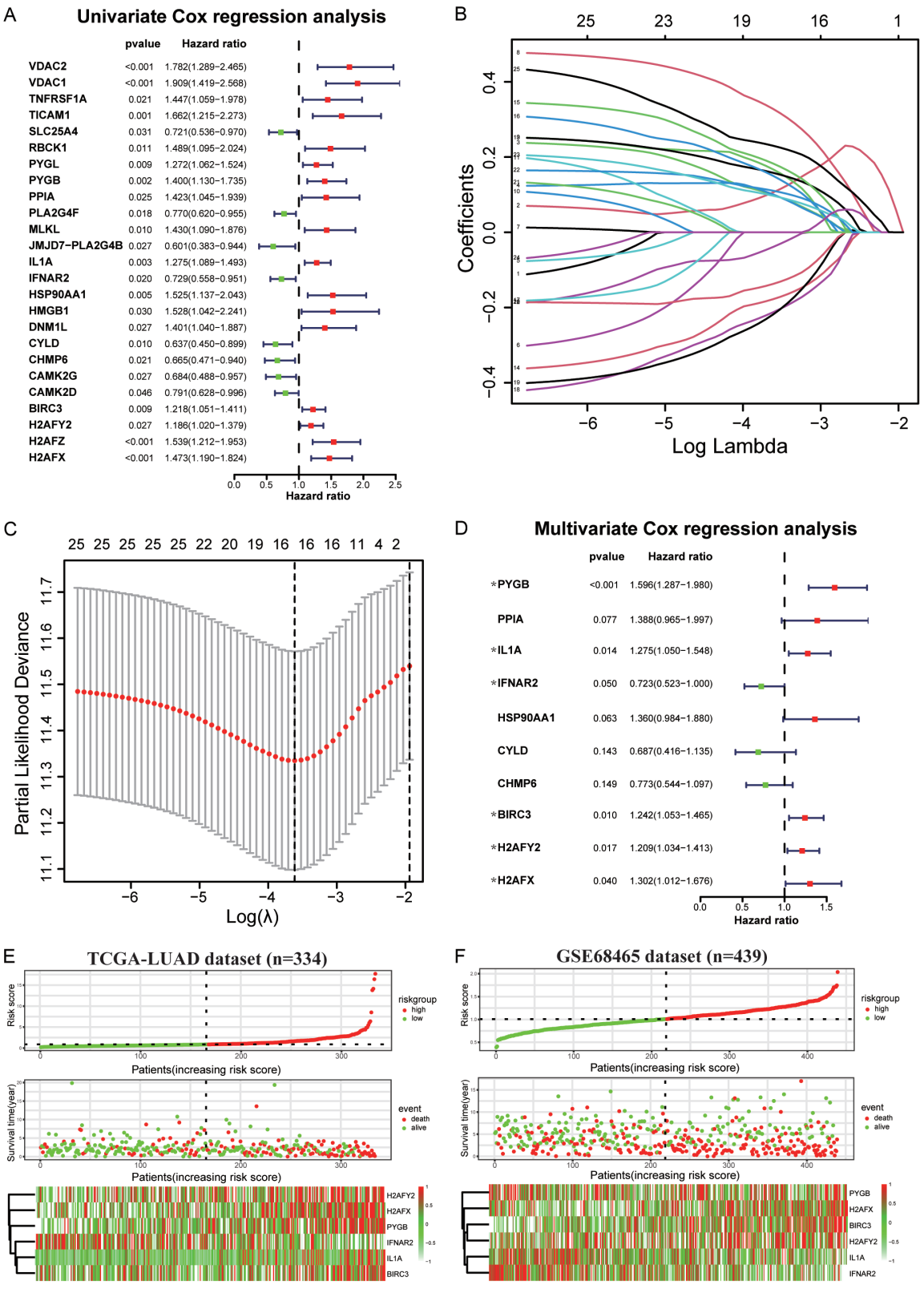

Figure 4. Development of a 6 NRG prognostic signature in the TCGA-LUAD cohort. A. Hazard ratio and *p*-value of NRGs related to the prognosis of LUAD, analyzed by univariate Cox regression. HR>1 (red) represented risk factors, while HR<1 (green) represented protective factors. B. LASSO coefficient spectrum of 25 NRGs related to the prognosis of LUAD. Generating a coefficient distribution map for a logarithmic (λ) sequence. C. Selecting the best

parameters for LUAD in the LASSO model (λ). D. Hazard ratio and *p*-value of NRGs related to the prognosis of LUAD, analyzed by multiple Cox regression. E, F. Distribution of the risk score, survival status, and survival time of LUAD, and the heatmaps of 6 NRGs related to LUAD patients' prognosis in the TCGA-LUAD and GSE68465 cohorts.

Table 4. Genes included in the NRG prognostic gene signature

Gene symbol	Full name	Coefficient	HR	95% CI	*p*-value
PYGB	Glycogen phosphorylase B	0.467771919	1.596433245	1.287-1.98	<0.001
BIRC3	Baculoviral IAP repeat-containing 3	0.216851481	1.242159604	1.053-1.465	0.010058719
IL1A	Interleukin 1 alpha	0.242869929	1.274902785	1.05-1.548	0.014046978
H2AFY2	H2A histone family member Y2	0.189604261	1.208771146	1.034-1.413	0.017389965
H2AFX	H2A histone family member X	0.263926113	1.30203199	1.012-1.676	0.040251954
IFNAR2	Interferon-alpha and beta receptor subunit 2	-0.324270834	0.723054388	0.523-1	0.049700296

The 6 NRG signature was an independent risk factor for the prognosis of LUAD

The validity of the prognostic model was evaluated in the TCGA-LUAD cohort (n = 334) and validated in the GSE68465 cohort (n = 439). We analyzed the relationship between risk score and clinicopathological data and found that the pT, pN, and pTNM stages in the high-risk score group were significantly higher than those in the low-risk score group (**Figure 5A-C**). Univariate Cox regression analysis revealed that the pT stage, pN stage, pM stage, pTNM stage, and risk score (HR = 1.324, 95% CI = 1.263-1.387, P<0.001) were risk factors for LUAD patients' OS (**Figure 5D**). After adjusting for these clinicopathological confounding variables above, multivariate Cox regression analysis showed that only the risk score was an independent indicator of OS for LUAD (HR = 1.220, 95% CI = 1.154-1.290, P<0.001) (**Figure 5E**). The Kaplan-Meier survival analysis showed that the OS of the high-risk score group in the TCGA-LUAD cohort was significantly shorter than that of the low-risk score group (median survival time = 2.2 years vs. 7.2 years, P<0.001) (**Figure 5F**). This was verified in the GSE68465 cohort (**Figure 5G**). The ROC curve showed that the Area Under Curve (AUC) of the risk scores in the TCGA-LUAD cohort (AUC = 0.842) and GSE68465 cohort (AUC = 0.790) were significantly larger than other clinicopathological factors (**Figure 5H**, **5I**).

The risk score based on the 6 NRG signature was associated with tumor immunity

Through gene set enrichment analysis (GSEA) of two risk score subgroups in the MSigDB collection (c5.all.v7.4.symbols.gmt), we identified many significant pathways related to immunity (Supplementary Figure 4A), including activation of the immune response, adaptive immune response, and T cell differentiation, which were down-regulated in the high-risk score group. The heatmap of immune infiltration showed that there was a significant difference in the infiltration abundance of 22 immune cells between the high-risk score group and the low-risk score group (Supplementary Figure 4B). Compared with other immune cells, the M2 macrophages were most significantly enriched in LUAD. ESTIMATE analysis showed that the ESTIMATEScore, ImmuneScore, and StromalScore in the high-risk score group were lower than those in the low-risk score group, but the TumorPurity was higher than that in the low-risk score group (**Figure 6A-D**). Necroptosis is involved in the TIME and anti-tumor immunity in a complex and important way [18, 22]. Therefore, we studied the correlation between the NRG signature and tumor immunity of LUAD. CIBERSORT analysis demonstrated that in the high-risk score group, the infiltration proportion of M1 macrophages, CD8 T, and activated NK cells was low, while the infiltration proportion of M2 macrophages and regulatory T cells was high (**Figure 6E**). The single-sample gene set enrichment analysis (ssGSEA) also showed that the relative abundance of most immunoactivated cells in the high-risk score group was lower, but the relative abundance of regulatory T and myeloid-derived suppressor cells (MDSC) cells was higher (**Figure 6F**).

We explored the correlation between risk score and immune checkpoints expression and found that many reported immunotherapy targets (PD-1, PD-L1, PD-L2, CTLA4, CD80, CD86, LAG3, TIM3, and TIGIT) had low expression lev-

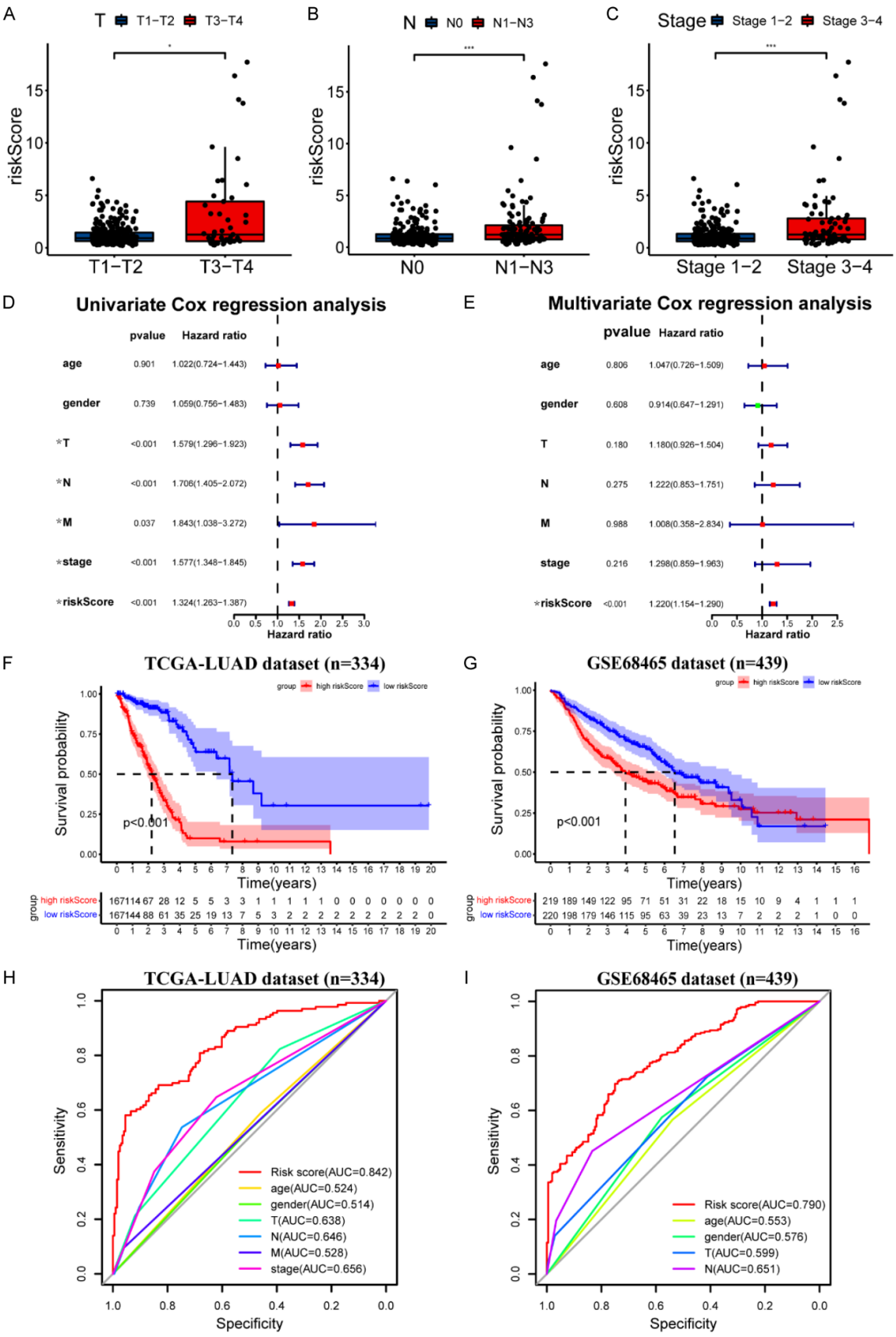
A
T T1–T2 T3–T4
riskScore
T1–T2
T3–T4
B
N N0 N1–N3
riskScore
N0
N1–N3
C
Stage Stage 1–2 Stage 3–4
riskScore
Stage 1–2
Stage 3–4
D
Univariate Cox regression analysis
pvalue Hazard ratio
age 0.901 1.022(0.724–1.443)
gender 0.739 1.059(0.756–1.483)
*T <0.001 1.579(1.296–1.923)
*N <0.001 1.706(1.405–2.072)
*M 0.037 1.843(1.038–3.272)
*stage <0.001 1.577(1.348–1.845)
*riskScore <0.001 1.324(1.263–1.387)
Hazard ratio
E
Multivariate Cox regression analysis
pvalue Hazard ratio
age 0.806 1.047(0.726–1.509)
gender 0.608 0.914(0.647–1.291)
T 0.180 1.180(0.926–1.504)
N 0.275 1.222(0.853–1.751)
M 0.988 1.008(0.358–2.834)
stage 0.216 1.298(0.859–1.963)
*riskScore <0.001 1.220(1.154–1.290)
Hazard ratio
F
TCGA-LUAD dataset (n=334)
group high riskScore low riskScore
Survival probability
p<0.001
Time(years)
high riskScore 167 114 67 28 12 5 5 3 3 1 1 1 1 1 0 0 0 0 0 0 0
low riskScore 167 144 88 61 35 25 19 13 7 5 3 2 2 2 2 2 2 2 2 0
G
GSE68465 dataset (n=439)
group high riskScore low riskScore
Survival probability
p<0.001
Time(years)
high riskScore 219 189 149 122 95 71 51 31 22 18 15 10 9 4 1 1 1
low riskScore 220 198 179 146 115 95 63 39 23 13 7 2 2 2 1 0 0
H
TCGA-LUAD dataset (n=334)
Sensitivity
Specificity
Risk score(AUC=0.842)
age(AUC=0.524)
gender(AUC=0.514)
T(AUC=0.638)
N(AUC=0.646)
M(AUC=0.528)
stage(AUC=0.656)
I
GSE68465 dataset (n=439)
Sensitivity
Specificity
Risk score(AUC=0.790)
age(AUC=0.553)
gender(AUC=0.576)
T(AUC=0.599)
N(AUC=0.651)

Figure 5. The 6 NRG signature was an independent risk factor for the prognosis of LUAD. A-C. Relationship between the risk score and clinicopathological parameters (pT stage, pN stage, and pTNM stage) in the TCGA-LUAD cohort. D, E. Forest maps of the risk score and clinicopathological parameters (age, gender, pT stage, pN stage, and pTNM stage), analyzed by univariate Cox regression and multiple Cox regression. F, G. Kaplan-Meier survival analysis of LUAD was stratified by the median risk score in the TCGA-LUAD and GSE68465 cohorts. H, I. ROC curves of the risk score and clinicopathological parameters for evaluating the prognosis of LUAD in the TCGA-LUAD and GSE68465 cohorts. *P<0.05, ***P<0.001.

els in the high-risk group (**Figure 6G-I**). The mutational landscape of the two groups was shown in Supplementary Figure 5, and the TMB level was lower in the high-risk score group than that in the low-risk score group (Supplementary Figure 5E). These results suggested that the high-risk score group had an immunosuppressive TME and might be tolerant to immunotherapy.

Clinical validation of 6 NRG signature in predicting LUAD prognosis and tumor immunity

In the clinical cohort, we calculated the risk score for each LUAD patient using the same method. We further explored the clinical value and practicability of the 6 NRG signature. In the clinical cohort, the pTNM stage and risk score in the immunotherapy-resistance group were significantly higher than those in the immunotherapy-response group (**Table 2**). A higher risk score was positively correlated to the higher pT, pN, and pTNM stages (**Figure 7A-C**). The median PFS in the low-risk score group was significantly better than that in the high-risk score group [not reached vs. 8.5 months, HR = 0.18, 95% CI: 0.04-0.72, P<0.001] (**Figure 7D**). RT-qPCR (**Figure 7E-G**) showed that the expression of immune cell markers and immune checkpoints in the high-risk score group was significantly lower than that in the low-risk score group. In the TCGA TARGET GTEx dataset (Supplementary Figure 6A) and clinical cohort (**Figure 7H**), *PYGB*, *IL1A*, *BIRC3*, *H2AFY2*, and *H2AFX* were highly expressed in LUAD, while *IFNAR2* was low expressed in LUAD. IHC (**Figure 7I**, Supplementary Figure 6B) showed that the expression of CD8 T cell markers (CD3 and CD8) was low, the expression of regulatory T cells marker (FOXP3) was high, and the expression of PD-1 related immune checkpoints (PD-1 and PD-L1) was low in the high-risk score group. The ORR of the low-risk score group was higher than that of the high-risk score group (60% vs. 30%, P = 0.37). In addition, a high-risk score was associated with tumor immunotherapy tolerance (**Figure 7J**). These results suggested that immunosuppression existed in the high-risk score group, and the efficacy of immunotherapy was poor.

The index of evaluating the sensitivity of immunotherapy is of great significance to guide the individualized treatment of LUAD. PD-L1 is one of the most common indicators to guide immunotherapy in LUAD [10]. By combining with risk score and PD-L1, the AUC for the LUAD immunotherapy sensitivity reached 0.808 (95% CI: 0.613-1.000) (**Figure 7K**). These results suggest that the 6 NRG signature plays a critical role in evaluating and predicting the prognosis and immunotherapy sensitivity in LUAD, which may guide the clinical individualized treatment of LUAD.

Development and validation of a predictive nomogram

Nomogram is based on multivariate Cox regression analysis and combined with multi-index to predict accurate clinical outcomes or the probability of the occurrence of certain events [37]. We combined the clinicopathological data of the TCGA-LUAD cohort with the 6 NRG prognostic signature to generate a predictive nomogram for predicting individual 1-year, 3-year, and 5-year survival probabilities of LUAD (C-index = 0.79, 95% CI = 0.75-0.82, P<0.001) (**Figure 8A**). The timeROC curve showed that the nomogram had a certain accuracy in predicting the 1-year OS (AUC = 0.821), 3-year OS (AUC = 0.840), and 5-year OS (AUC = 0.809) of LUAD in the training and validation sets (**Figure 8B**, **8C**). The 1-year, 3-year, and 5-year calibration curves of the training and validation sets revealed a favorable match between the actual and predicted probability of OS (**Figure 8D**, **8E**).

Discussion

Although mutations in tumorigenic driver genes of LUAD are common, the TMB level, PD-L1 expression level, and immune cell infiltration degree are low, which leads to poor immuno-

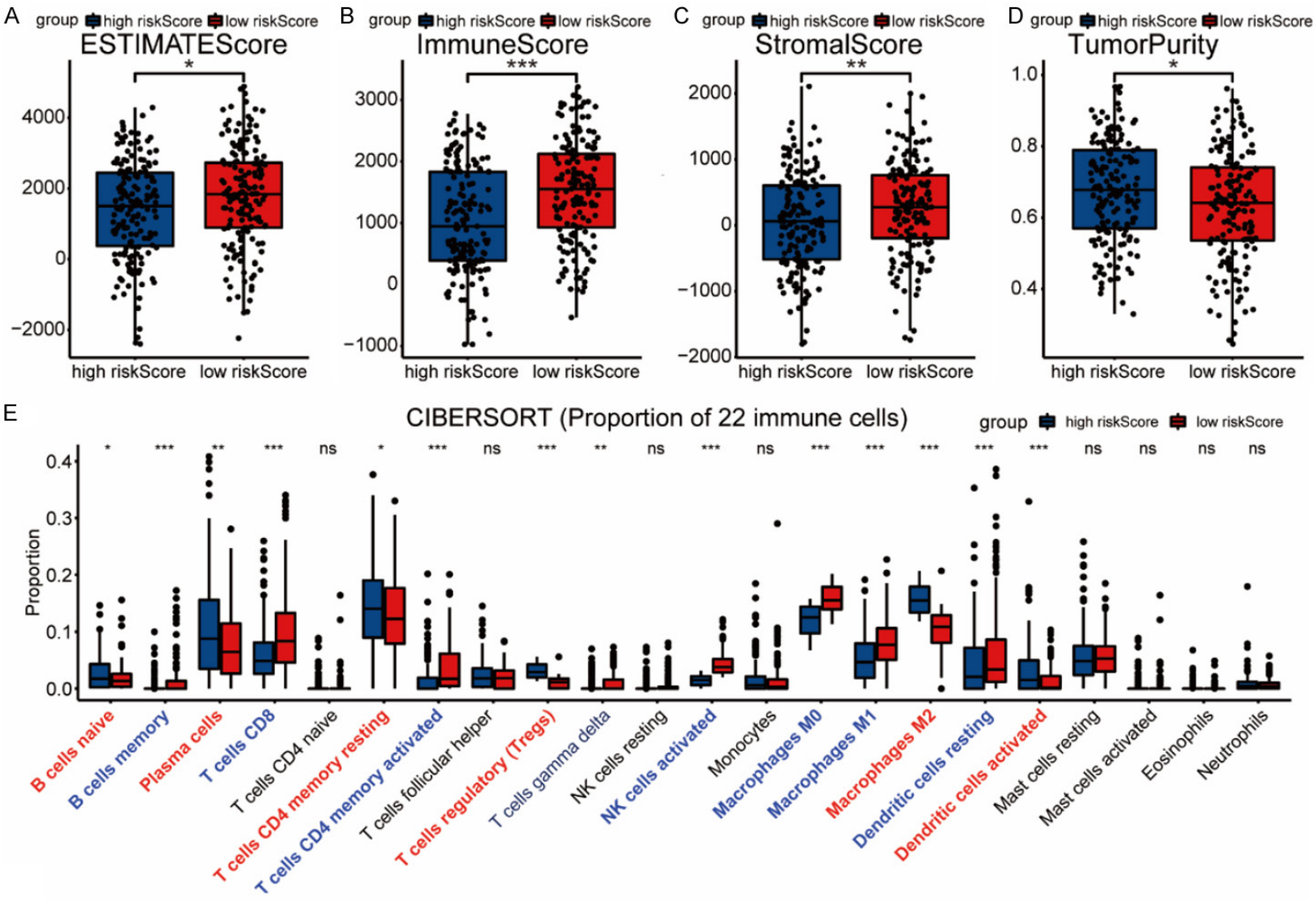
A
group high riskScore low riskScore
ESTIMATEScore
*
4000
2000
0
−2000
high riskScore low riskScore
B
group high riskScore low riskScore
ImmuneScore
***
3000
2000
1000
0
−1000
high riskScore low riskScore
C
group high riskScore low riskScore
StromalScore
**
2000
1000
0
−1000
−2000
high riskScore low riskScore
D
group high riskScore low riskScore
TumorPurity
*
1.0
0.8
0.6
0.4
high riskScore low riskScore
E
CIBERSORT (Proportion of 22 immune cells)
group high riskScore low riskScore
Proportion
0.4
0.3
0.2
0.1
0.0
B cells naive
B cells memory
Plasma cells
T cells CD8
T cells CD4 naive
T cells CD4 memory resting
T cells CD4 memory activated
T cells follicular helper
T cells regulatory (Tregs)
T cells gamma delta
NK cells resting
NK cells activated
Monocytes
Macrophages M0
Macrophages M1
Macrophages M2
Dendritic cells resting
Dendritic cells activated
Mast cells resting
Mast cells activated
Eosinophils
Neutrophils

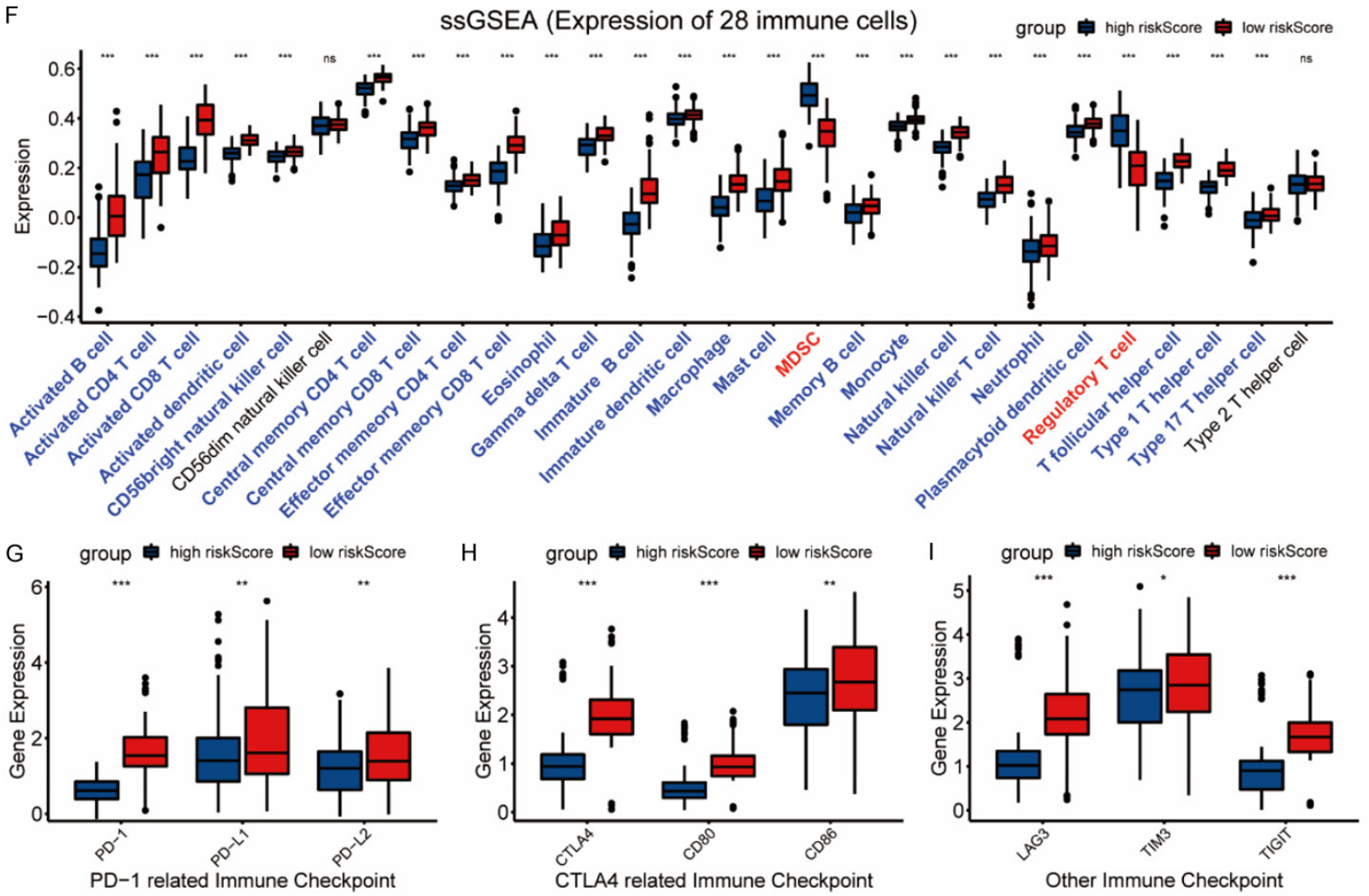

Figure 6. The NRG signature was associated with tumor immunity. Comparison of the ESTIMATEScore (A), ImmuneScore (B), StromalScore (C), and TumorPurity (D) between two risk score subgroups in the TCGA-LUAD cohort. Comparison analysis of the proportion of immune cells (E), expression of immune cells (F), PD-1 related immune checkpoints (PD-1, PD-L1, and PD-L2) (G), CTLA4 related immune checkpoints (CTLA4, CD80, and CD86) (H), and other immune checkpoints (LAG3, TIM3, and TIGIT) (I) of LUAD between two risk-score subgroups in the TCGA-LUAD cohort. ns: no significance, *P<0.05, **P<0.01, ***P<0.001.

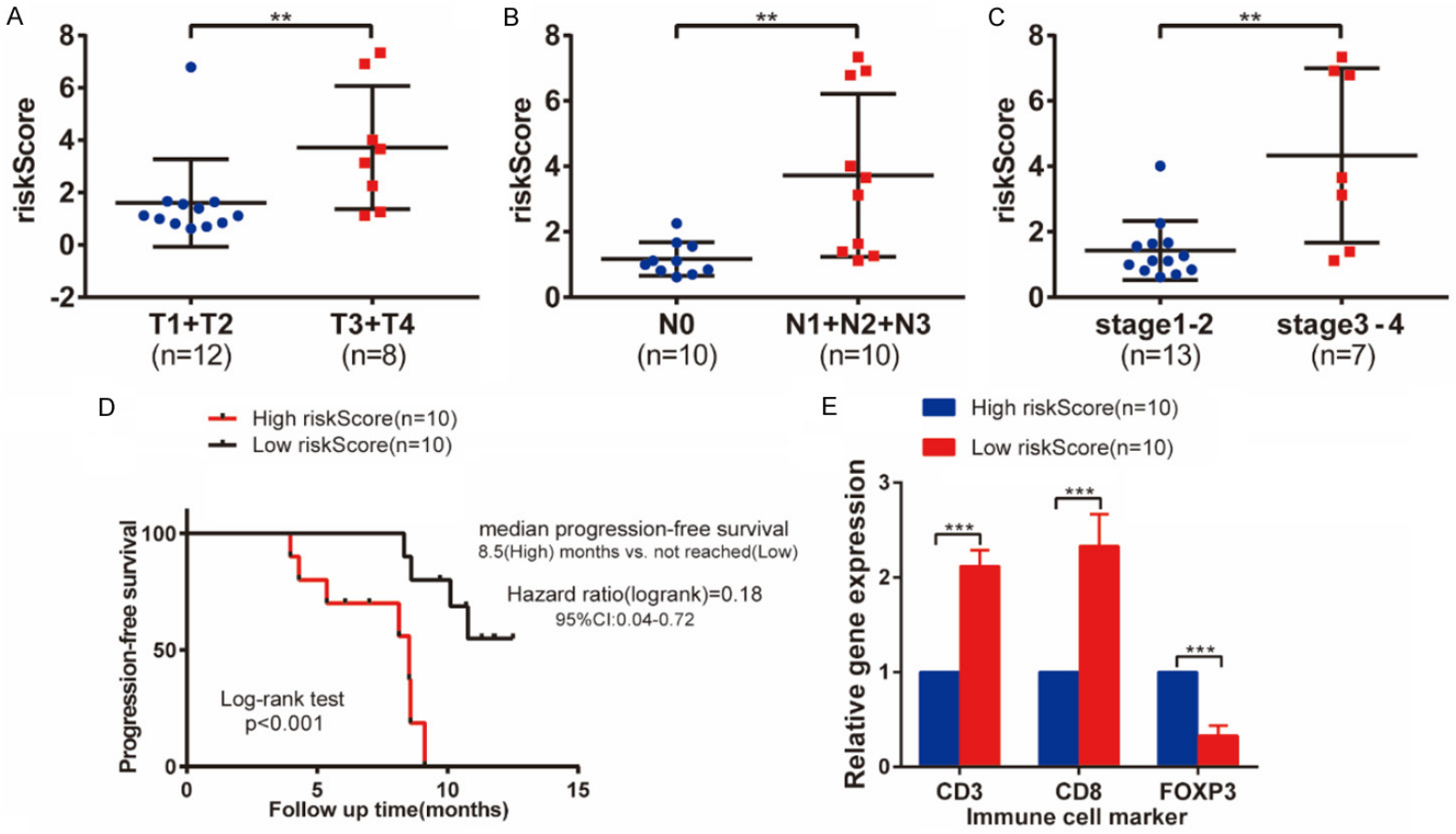
A
**
riskScore
8
6
4
2
0
-2
T1+T2
(n=12)
T3+T4
(n=8)
B
**
riskScore
8
6
4
2
0
N0
(n=10)
N1+N2+N3
(n=10)
C
**
riskScore
8
6
4
2
0
stage1-2
(n=13)
stage3 - 4
(n=7)
D
High riskScore(n=10)
Low riskScore(n=10)
median progression-free survival
8.5(High) months vs. not reached(Low)
Hazard ratio(logrank)=0.18
95%CI:0.04-0.72
Log-rank test
p<0.001
Progression-free survival
100
50
0
0
5
10
15
Follow up time(months)
E
High riskScore(n=10)
Low riskScore(n=10)
Relative gene expression
3
2
1
0
***
***
***
CD3
CD8
FOXP3
Immune cell marker

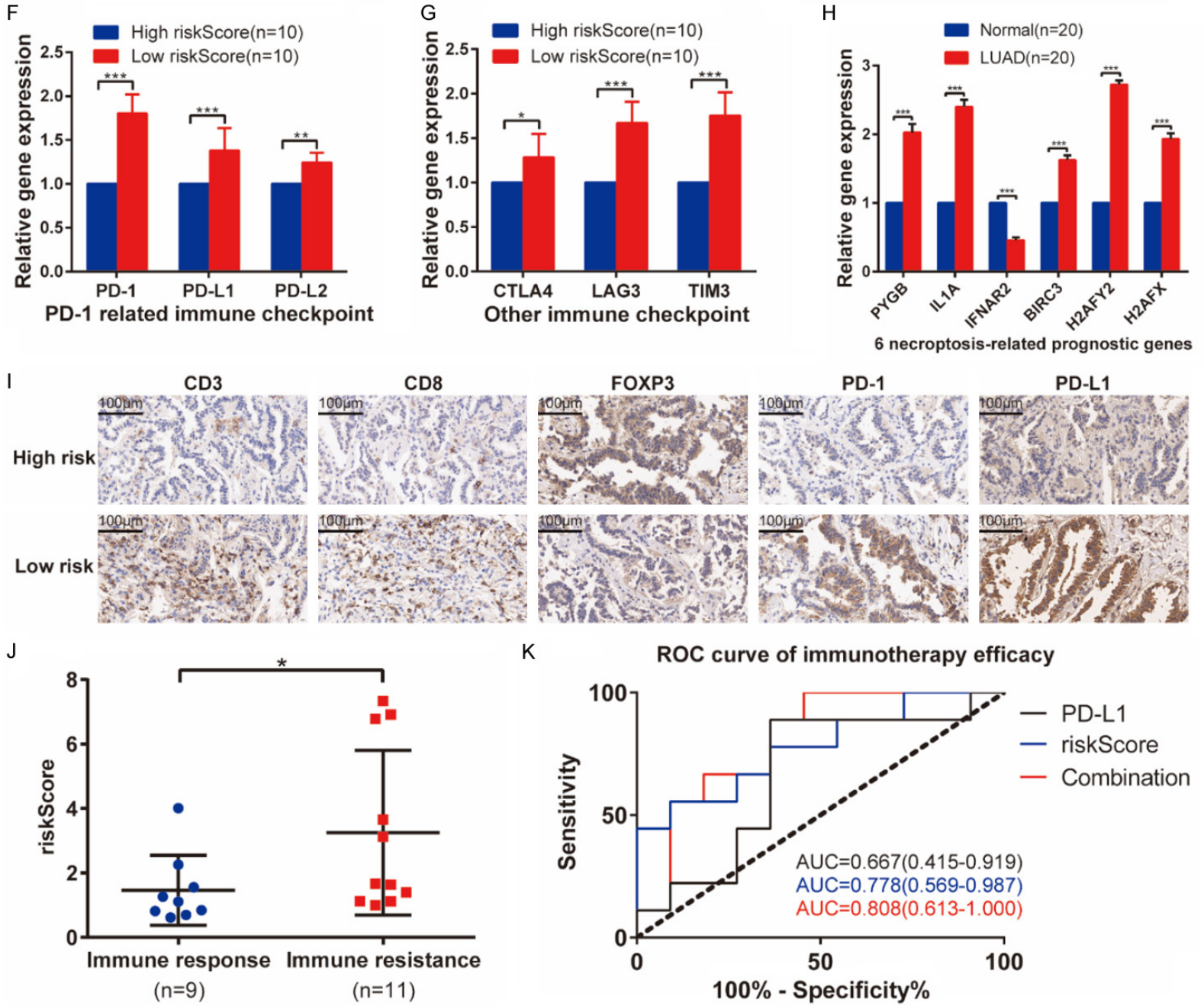
F
High riskScore(n=10)
Low riskScore(n=10)
Relative gene expression
PD-1
PD-L1
PD-L2
PD-1 related immune checkpoint
G
High riskScore(n=10)
Low riskScore(n=10)
Relative gene expression
CTLA4
LAG3
TIM3
Other immune checkpoint
H
Normal(n=20)
LUAD(n=20)
Relative gene expression
PYGB
IL1A
IFNAR2
BIRC3
H2AFY2
H2AFX
6 necroptosis-related prognostic genes
I
CD3
CD8
FOXP3
PD-1
PD-L1
High risk
Low risk
100μm
J
riskScore
Immune response
(n=9)
Immune resistance
(n=11)
K
ROC curve of immunotherapy efficacy
Sensitivity
100% - Specificity%
PD-L1
riskScore
Combination
AUC=0.667(0.415-0.919)
AUC=0.778(0.569-0.987)
AUC=0.808(0.613-1.000)

Figure 7. Clinical validation of the 6 NRG signature. A-C. Relationship between the risk score and clinicopathological parameters (pT stage, pN stage, and pTNM stage) in the clinical cohort. D. Statistical analysis of the association of risk score with PFS in LUAD patients. E. Comparison of the mRNA expression of immune cell markers between the two risk score subgroups by RT-qPCR. F, G. Comparison of the mRNA expression in PD-1-related and other immune checkpoints between the two risk score subgroups by RT-qPCR. H. Comparison of the expression levels of 6 necroptosis-related prognostic genes between LUAD and normal lung tissues in the clinical cohort. I. Comparison of the protein expression of immune cell markers and immune checkpoints between the two groups by IHC. Scale bars: 100 μm. J. Comparison of risk scores between the immunotherapy resistance group and immunotherapy response group. K. Comparison of ROC curves of risk score, PD-L1, and the combination of risk score, PD-L1 for evaluating the immunotherapy sensitivity. PFS: Progression-Free Survival, *P<0.05, **P<0.01, ***P<0.001.

therapy efficacy of LUAD [38]. Therefore, finding effective biomarkers is crucial for promoting LUAD immunotherapy.

Like apoptosis, pyroptosis, and ferroptosis, necroptosis is one pattern of programmed cell death, which has the morphological characteristics of necrotic cell death. Cell rupture and death caused by necroptosis can replace apoptosis, promote tumor cell death, activate congenital and adaptive immune responses, and enhance anti-tumor immunity, which makes necroptosis a target for tumor prognosis and treatment [14]. Moreover, chronic necroptosis-induced inflammation has been linked to cancer metastasis and immunosuppression [18, 39]. However, necroptosis has been proven to have dual effects on the progression and prognosis of many cancers [40, 41]. Owing to the significance of necroptosis in lung cancer, we reasonably speculate that NRGs have an extensive prospect in predicting the prognosis and tumor immunity of LUAD.

The 28 necroptosis-related DEGs were mainly enriched in cell growth regulation, programmed necrotic cell death, necroptosis, JAK-STAT signaling pathway, and immune cell differentiation. Interestingly, the expression of necroptosis markers such as *RIPK1*, *RIPK3*, *MLKL*, and *TLR4* in LUAD cell lines and tissues was significantly lower than those in normal cell lines and tissues, which corresponded to the previous studies [25, 26]. Furthermore, the JAK-STAT signaling pathway has been shown to play an important role in tumor inflammation and lung carcinogenesis [42, 43]. These results suggested that necroptosis was related to the tumorigenesis and tumor immunity of LUAD.

A gene signature related to a signal pathway or biological process has been shown to have prognostic significance in a variety of cancers [44, 45]. In our study, a 6 NRG prognostic signature (*PYGB*, *IL1A*, *IFNAR2*, *BIRC3*, *H2AFY2*, and *H2AFX*) was established by multivariate Cox regression analysis. Interestingly, previous studies have shown that these genes play an important role in regulating the progression and prognosis of many cancers. PYGB has been reported to be associated with the occurrence and progression of hepatocellular carcinoma [46], ovarian cancer [47], and NSCLC [48]. IL1A has been linked to inflammatory diseases, cancer, and immunotherapy resistance [49, 50]. Multiple studies on population-based or clinical trial cohorts have demonstrated that the expression and mutation of *BIRC3* could predict the progression and chemosensitivity of hematological diseases, especially in chronic lymphoblastic leukemia (CLL) [51, 52]. The expression of *H2AFX* was a diagnostic index of LUAD related to poor prognosis [53]. In addition to regulating antiviral and tumor immunity [54], *IFNAR2* has been considered to be an independent prognostic factor for PFS and OS in lung cancer [55]. Therefore, the combination of these genes might take an unexpected effect in optimizing the prognostic evaluation strategy of LUAD.

Immune infiltration in the TME has an important influence on the clinical features and prognosis of NSCLC [56, 57]. In most subtypes of tumor-infiltrating immune cells, CD8 T cells are the most important index to evaluate anti-tumor immunity and have the greatest influence on the prognosis of patients [58]. Besides, the anti-inflammatory and immunosuppressive functions of regulatory T cells [59] and M2 macrophages [60] played an important role in tumorigenesis, tumor development, and drug resistance to immunotherapy. ICIs can improve the innate anti-tumor immunity, and induce strong and lasting clinical responses in NSCLC patients, making individuals more likely to benefit clinically [61]. We divided the TCGA cohort into two subgroups by median risk score, which is an independent risk factor for LUAD. We

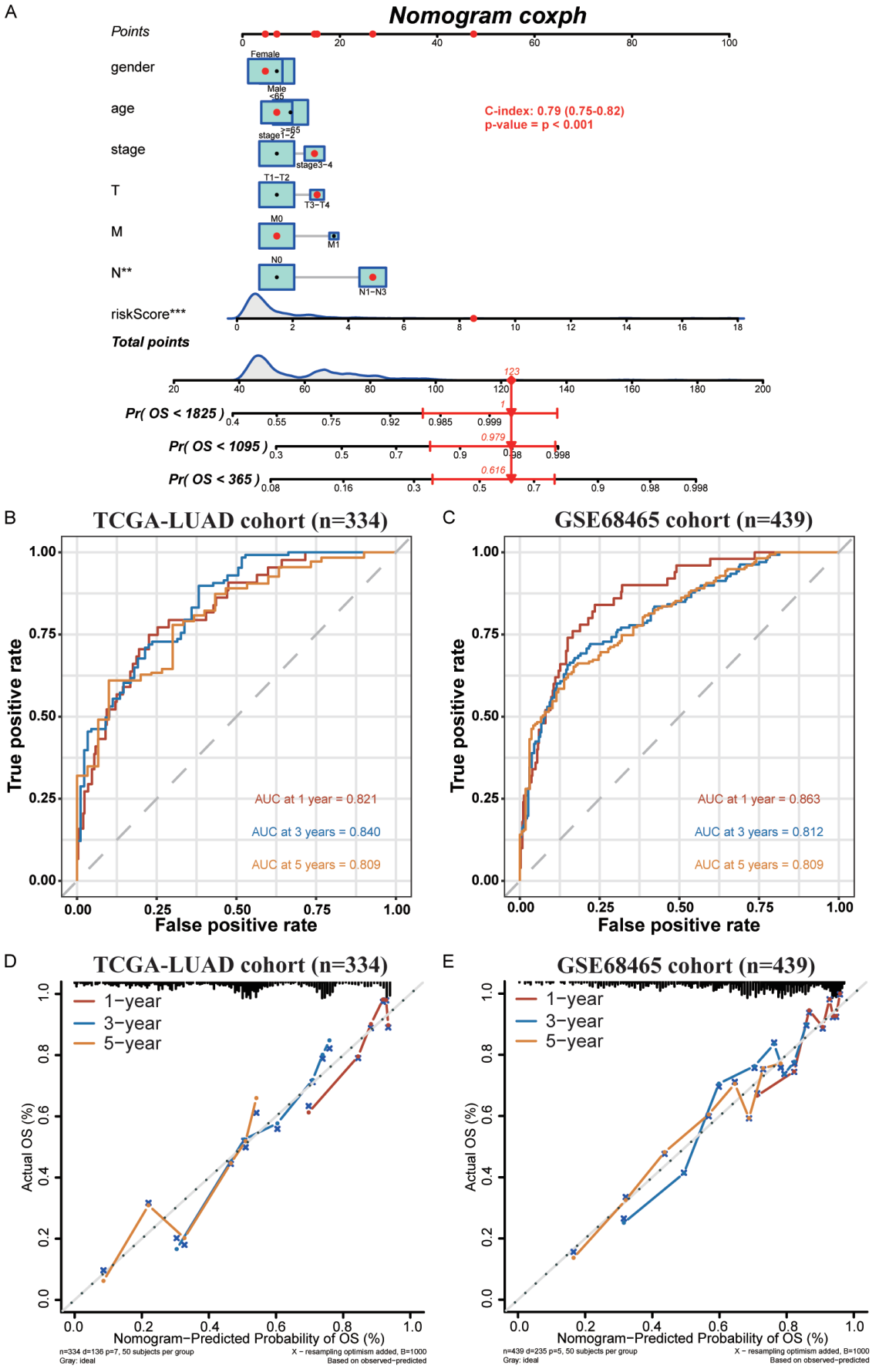
A
Nomogram coxph
Points
gender
Female
Male
age
<65
>=65
stage
stage1−2
stage3−4
T
T1−T2
T3−T4
M
M0
M1
N**
N0
N1−N3
riskScore***
Total points
Pr(OS < 1825)
Pr(OS < 1095)
Pr(OS < 365)
C-index: 0.79 (0.75-0.82)
p-value = p < 0.001
B
TCGA-LUAD cohort (n=334)
True positive rate
False positive rate
AUC at 1 year = 0.821
AUC at 3 years = 0.840
AUC at 5 years = 0.809
C
GSE68465 cohort (n=439)
AUC at 1 year = 0.863
AUC at 3 years = 0.812
AUC at 5 years = 0.809
D
TCGA-LUAD cohort (n=334)
1−year
3−year
5−year
Actual OS (%)
Nomogram−Predicted Probability of OS (%)
n=334 d=136 p=7, 50 subjects per group
Gray: ideal
X − resampling optimism added, B=1000
Based on observed−predicted
E
GSE68465 cohort (n=439)
n=439 d=235 p=5, 50 subjects per group

Figure 8. Development and validation of a predictive nomogram. A. Nomogram of the TCGA-LUAD cohort (training set) was used to predict the 1-year, 3-year, and 5-year overall survival rate. B, C. The timeROC curve of nomogram model for evaluating OS of LUAD in training and validation sets. D, E. The 1-year, 3-year, and 5-year calibration curves of the nomogram model in training and validation sets.

found that all DEGs were enriched in the immunomodulatory pathway, including activation of the immune response, adaptive immune response, and T cell differentiation. In the training set, we found that high-risk scores based on the 6 NRG signature were associated with poor prognosis, weak immune infiltration (M1 macrophages, CD8 T, and activated NK cells), strong immunosuppression (M2 macrophages and regulatory T cells) and low expression of immune checkpoints (PD-1, PD-L1, PD-L2, CTLA4, CD80, CD86, LAG3, TIM3, and TIGIT). Therefore, the high-risk group has low immune activity and is less likely to benefit from immunotherapy.

In the clinical cohort, we calculated the risk score for each LUAD patient. The high-risk score group had higher pT, pN, and pTNM stages, but shorter PFS. In the high-risk score group, the expression of immune activation regulatory targets and immune checkpoints was down-regulated, and the expression of immunosuppression regulatory targets was up-regulated. In addition, the combination of risk score and PD-L1 can better predict the sensitivity of immunotherapy. Interestingly, a study has shown that induction of necroptosis and ICIs had a synergistic effect in anti-tumor therapy [62]. Therefore, the risk score based on the 6 NRG signature was closely related to tumor immune infiltration and immunotherapy sensitivity of LUAD and was expected to become their predictive marker.

To better predict the probability of individual OS, we developed a nomogram with other clinicopathological data and the NRG prognosis signature to predict the probability of 1-year OS, 3-year OS, and 5-year OS in LUAD patients. The c-index, ROC curve, and calibration curve of the nomogram proved that the prognostic model had a good performance in predicting the OS of LUAD. Therefore, we constructed and validated a nomogram that could well predict the probability of short-term OS in LUAD.

Our research has some limitations. First, this is a retrospective study with inherent selection bias; Second, the association between the NRG signature and LUAD immune infiltration still needs to be confirmed in vitro; Third, due to the lack of sufficient clinical samples, only a small number of clinical cases were used to verify the role of the NRG signature in predicting immunotherapy sensitivity and only the GEO dataset was used to verify the effectiveness in the nomogram prognostic model.

Conclusion

Through comprehensive and systematic bioinformatics analysis, we identified a 6 NRG signature related to the prognosis and tumor immunity of LUAD and verified it in the GEO and clinical cohorts. More importantly, we created and verified a nomogram that can effectively predict the OS of LUAD patients. These results complement and optimize the prognostic evaluation system of LUAD and may be helpful to the individualized clinical decision-making of LUAD immunotherapy.

Acknowledgements

This study was supported by grants from The National Natural Science Foundation of China (No. 81871886, 81672415, 82073121), The Natural Science Foundation of Guangdong Province (No. 2017A030313474), Guangdong Science and Technology Department (No. 2017B030314026), Guangdong Basic and Applied Basic Research Foundation (No. 2020A1515010041), Guangzhou Science and Technology Project (No. 202103000063) and The Fundamental Research Funds for The Central Universities (No. 19ykpy110).

Disclosure of conflict of interest

None.

Address correspondence to: Huayue Lin and Minghui Wang, Guangdong Provincial Key Laboratory of Malignant Tumor Epigenetics and Gene Regulation, Sun Yat-sen Memorial Hospital, Sun Yat-sen University, Guangzhou, Guangdong, China. E-mail: linhy29@mail.sysu.edu.cn (HYL); wmingh@mail.sysu.edu.cn (MHW)

References

[1] Miller KD, Nogueira L, Mariotto AB, Rowland JH, Yabroff KR, Alfano CM, Jemal A, Kramer JL and Siegel RL. Cancer treatment and survivorship statistics, 2019. CA Cancer J Clin 2019; 69: 363-385.

[2] DeSantis CE, Miller KD, Goding Sauer A, Jemal A and Siegel RL. Cancer statistics for African Americans, 2019. CA Cancer J Clin 2019; 69: 211-233.

[3] Sung H, Ferlay J, Siegel RL, Laversanne M, Soerjomataram I, Jemal A and Bray F. Global cancer statistics 2020: GLOBOCAN estimates of incidence and mortality worldwide for 36 cancers in 185 countries. CA Cancer J Clin 2021; 71: 209-249.

[4] Neal RD, Hamilton W and Rogers TK. Lung cancer. BMJ 2014; 349: g6560.

[5] Hirsch FR, Scagliotti GV, Mulshine JL, Kwon R, Curran WJ Jr, Wu YL and Paz-Ares L. Lung cancer: current therapies and new targeted treatments. Lancet 2017; 389: 299-311.

[6] Camidge DR, Doebele RC and Kerr KM. Comparing and contrasting predictive biomarkers for immunotherapy and targeted therapy of NSCLC. Nat Rev Clin Oncol 2019; 16: 341-355.

[7] Sharma P, Hu-Lieskovan S, Wargo JA and Ribas A. Primary, adaptive, and acquired resistance to cancer immunotherapy. Cell 2017; 168: 707-723.

[8] Jiang P, Gu S, Pan D, Fu J, Sahu A, Hu X, Li Z, Traugh N, Bu X, Li B, Liu J, Freeman GJ, Brown MA, Wucherpfennig KW and Liu XS. Signatures of T cell dysfunction and exclusion predict cancer immunotherapy response. Nat Med 2018; 24: 1550-1558.

[9] Abu Hejleh T, Furqan M, Ballas Z and Clamon G. The clinical significance of soluble PD-1 and PD-L1 in lung cancer. Crit Rev Oncol Hematol 2019; 143: 148-152.

[10] Tian Y, Zhai X, Yan W, Zhu H and Yu J. Clinical outcomes of immune checkpoint blockades and the underlying immune escape mechanisms in squamous and adenocarcinoma NSCLC. Cancer Med 2021; 10: 3-14.

[11] Christofferson DE and Yuan J. Necroptosis as an alternative form of programmed cell death. Curr Opin Cell Biol 2010; 22: 263-268.

[12] Fulda S. The mechanism of necroptosis in normal and cancer cells. Cancer Biol Ther 2013; 14: 999-1004.

[13] Li J, McQuade T, Siemer AB, Napetschnig J, Moriwaki K, Hsiao YS, Damko E, Moquin D, Walz T, McDermott A, Chan FK and Wu H. The RIP1/RIP3 necrosome forms a functional amyloid signaling complex required for programmed necrosis. Cell 2012; 150: 339-350.

[14] Gong Y, Fan Z, Luo G, Yang C, Huang Q, Fan K, Cheng H, Jin K, Ni Q, Yu X and Liu C. The role of necroptosis in cancer biology and therapy. Mol Cancer 2019; 18: 100.

[15] Brault M and Oberst A. Controlled detonation: evolution of necroptosis in pathogen defense. Immunol Cell Biol 2017; 95: 131-136.

[16] Tang R, Xu J, Zhang B, Liu J, Liang C, Hua J, Meng Q, Yu X and Shi S. Ferroptosis, necroptosis, and pyroptosis in anticancer immunity. J Hematol Oncol 2020; 13: 110.

[17] Grivennikov SI, Greten FR and Karin M. Immunity, inflammation, and cancer. Cell 2010; 140: 883-899.

[18] Seifert L, Werba G, Tiwari S, Giao Ly NN, Alothman S, Alqunaibit D, Avanzi A, Barilla R, Daley D, Greco SH, Torres-Hernandez A, Pergamo M, Ochi A, Zambirinis CP, Pansari M, Rendon M, Tippens D, Hundeyin M, Mani VR, Hajdu C, Engle D and Miller G. The necrosome promotes pancreatic oncogenesis via CXCL1 and Mincle-induced immune suppression. Nature 2016; 532: 245-249.

[19] Stoll G, Ma Y, Yang H, Kepp O, Zitvogel L and Kroemer G. Pro-necrotic molecules impact local immunosurveillance in human breast cancer. Oncoimmunology 2017; 6: e1299302.

[20] Geserick P, Wang J, Schilling R, Horn S, Harris PA, Bertin J, Gough PJ, Feoktistova M and Leverkus M. Absence of RIPK3 predicts necroptosis resistance in malignant melanoma. Cell Death Dis 2015; 6: e1884.

[21] Park S, Hatanpaa KJ, Xie Y, Mickey BE, Madden CJ, Raisanen JM, Ramnarain DB, Xiao G, Saha D, Boothman DA, Zhao D, Bachoo RM, Pieper RO and Habib AA. The receptor interacting protein 1 inhibits p53 induction through NF-kappaB activation and confers a worse prognosis in glioblastoma. Cancer Res 2009; 69: 2809-2816.

[22] Feng X, Song Q, Yu A, Tang H, Peng Z and Wang X. Receptor-interacting protein kinase 3 is a predictor of survival and plays a tumor suppressive role in colorectal cancer. Neoplasma 2015; 62: 592-601.

[23] Wang Q, Chen W, Xu X, Li B, He W, Padilla MT, Jang JH, Nyunoya T, Amin S, Wang X and Lin Y. RIP1 potentiates BPDE-induced transformation in human bronchial epithelial cells through catalase-mediated suppression of excessive reactive oxygen species. Carcinogenesis 2013; 34: 2119-2128.

[24] Kim J, Chung JY, Park YS, Jang SJ, Kim HR, Choi CM and Song JS. Prognostic significance of CHIP and RIPK3 in non-small cell lung cancer. Cancers (Basel) 2020; 12: 1496.

[25] Wang Q, Wang P, Zhang L, Tessema M, Bai L, Xu X, Li Q, Zheng X, Saxton B, Chen W, Willink R, Li Z, Zhang L, Belinsky SA, Wang X, Zhou B

and Lin Y. Epigenetic regulation of RIP3 suppresses necroptosis and increases resistance to chemotherapy in non-small cell lung cancer. Transl Oncol 2020; 13: 372-382.
[26] Park JE, Lee JH, Lee SY, Hong MJ, Choi JE, Park S, Jeong JY, Lee EB, Choi SH, Lee YH, Seo HW, Yoo SS, Lee J, Cha SI, Kim CH and Park JY. Expression of key regulatory genes in necroptosis and its effect on the prognosis in non-small cell lung cancer. J Cancer 2020; 11: 5503-5510.
[27] Feng H, Zhong L, Yang X, Wan Q, Pei X and Wang J. Development and validation of prognostic index based on autophagy-related genes in patient with head and neck squamous cell carcinoma. Cell Death Discov 2020; 6: 59.
[28] Gao X, Tang M, Tian S, Li J and Liu W. A ferroptosis-related gene signature predicts overall survival in patients with lung adenocarcinoma. Future Oncol 2021; 17: 1533-1544.
[29] Dong Z, Bian L, Wang M, Wang L and Wang Y. Identification of a pyroptosis-related gene signature for prediction of overall survival in lung adenocarcinoma. J Oncol 2021; 2021: 6365459.
[30] Simon N, Friedman J, Hastie T and Tibshirani R. Regularization paths for Cox's proportional hazards model via coordinate descent. J Stat Softw 2011; 39: 1-13.
[31] Yoshihara K, Shahmoradgoli M, Martínez E, Vegesna R, Kim H, Torres-Garcia W, Treviño V, Shen H, Laird PW, Levine DA, Carter SL, Getz G, Stemke-Hale K, Mills GB and Verhaak RG. Inferring tumour purity and stromal and immune cell admixture from expression data. Nat Commun 2013; 4: 2612.
[32] Hänzelmann S, Castelo R and Guinney J. GSVA: gene set variation analysis for microarray and RNA-seq data. BMC Bioinformatics 2013; 14: 7.
[33] Eisenhauer EA, Therasse P, Bogaerts J, Schwartz LH, Sargent D, Ford R, Dancey J, Arbuck S, Gwyther S, Mooney M, Rubinstein L, Shankar L, Dodd L, Kaplan R, Lacombe D and Verweij J. New response evaluation criteria in solid tumours: revised RECIST guideline (version 1.1). Eur J Cancer 2009; 45: 228-247.
[34] Wang W, Wu D, He X, Hu X, Hu C, Shen Z, Lin J, Pan Z, He Z, Lin H and Wang M. CCL18-induced HOTAIR upregulation promotes malignant progression in esophageal squamous cell carcinoma through the miR-130a-5p-ZEB1 axis. Cancer Lett 2019; 460: 18-28.
[35] Jouan-Lanhouet S, Riquet F, Duprez L, Vanden Berghe T, Takahashi N and Vandenabeele P. Necroptosis, in vivo detection in experimental disease models. Semin Cell Dev Biol 2014; 35: 2-13.
[36] Kaiser WJ, Sridharan H, Huang C, Mandal P, Upton JW, Gough PJ, Sehon CA, Marquis RW, Bertin J and Mocarski ES. Toll-like receptor 3-mediated necrosis via TRIF, RIP3, and MLKL. J Biol Chem 2013; 288: 31268-31279.
[37] Balachandran VP, Gonen M, Smith JJ and DeMatteo RP. Nomograms in oncology: more than meets the eye. Lancet Oncol 2015; 16: e173-180.
[38] Aarreberg LD, Esser-Nobis K, Driscoll C, Shuvarikov A, Roby JA and Gale M Jr. Interleukin-1β induces mtDNA release to activate innate immune signaling via cGAS-STING. Mol Cell 2019; 74: 801-815.e806.
[39] Strilic B, Yang L, Albarrán-Juárez J, Wachsmuth L, Han K, Müller UC, Pasparakis M and Offermanns S. Tumour-cell-induced endothelial cell necroptosis via death receptor 6 promotes metastasis. Nature 2016; 536: 215-218.
[40] Wang T, Jin Y, Yang W, Zhang L, Jin X, Liu X, He Y and Li X. Necroptosis in cancer: an angel or a demon? Tumour Biol 2017; 39: 1010428317711539.
[41] Qin X, Ma D, Tan YX, Wang HY and Cai Z. The role of necroptosis in cancer: a double-edged sword? Biochim Biophys Acta Rev Cancer 2019; 1871: 259-266.
[42] Buchert M, Burns CJ and Ernst M. Targeting JAK kinase in solid tumors: emerging opportunities and challenges. Oncogene 2016; 35: 939-951.
[43] Grabner B, Schramek D, Mueller KM, Moll HP, Svinka J, Hoffmann T, Bauer E, Blaas L, Hruschka N, Zboray K, Stiedl P, Nivarthi H, Bogner E, Gruber W, Mohr T, Zwick RH, Kenner L, Poli V, Aberger F, Stoiber D, Egger G, Esterbauer H, Zuber J, Moriggl R, Eferl R, Győrffy B, Penninger JM, Popper H and Casanova E. Disruption of STAT3 signalling promotes KRAS-induced lung tumorigenesis. Nat Commun 2015; 6: 6285.
[44] Karamichalis R, Kari L, Konstantinidis S, Kopecki S and Solis-Reyes S. Additive methods for genomic signatures. BMC Bioinformatics 2016; 17: 313.
[45] Li N, Wang J and Zhan X. Identification of immune-related gene signatures in lung adenocarcinoma and lung squamous cell carcinoma. Front Immunol 2021; 12: 752643.
[46] Cui G, Wang H, Liu W, Xing J, Song W, Zeng Z, Liu L, Wang H, Wang X, Luo H, Leng X and Shen S. Glycogen phosphorylase B is regulated by miR101-3p and promotes hepatocellular carcinoma tumorigenesis. Front Cell Dev Biol 2020; 8: 566494.
[47] Zhou Y, Jin Z and Wang C. Glycogen phosphorylase B promotes ovarian cancer progression via Wnt/β-catenin signaling and is regulated by

miR-133a-3p. Biomed Pharmacother 2019; 120: 109449.
[48] Xiao L, Wang W, Huangfu Q, Tao H and Zhang J. PYGB facilitates cell proliferation and invasiveness in non-small cell lung cancer by activating the Wnt-β-catenin signaling pathway. Biochem Cell Biol 2020; 98: 565-574.
[49] Malik A and Kanneganti TD. Function and regulation of IL-1α in inflammatory diseases and cancer. Immunol Rev 2018; 281: 124-137.
[50] Lim SY, Lee JH, Gide TN, Menzies AM, Guminski A, Carlino MS, Breen EJ, Yang JYH, Ghazanfar S, Kefford RF, Scolyer RA, Long GV and Rizos H. Circulating cytokines predict immune-related toxicity in melanoma patients receiving anti-PD-1-based immunotherapy. Clin Cancer Res 2019; 25: 1557-1563.
[51] Asslaber D, Wacht N, Leisch M, Qi Y, Maeding N, Hufnagl C, Jansko B, Zaborsky N, Villunger A, Hartmann TN, Greil R and Egle A. BIRC3 expression predicts CLL progression and defines treatment sensitivity via enhanced NF-κB nuclear translocation. Clin Cancer Res 2019; 25: 1901-1912.
[52] Landau DA, Carter SL, Stojanov P, McKenna A, Stevenson K, Lawrence MS, Sougnez C, Stewart C, Sivachenko A, Wang L, Wan Y, Zhang W, Shukla SA, Vartanov A, Fernandes SM, Saksena G, Cibulskis K, Tesar B, Gabriel S, Hacohen N, Meyerson M, Lander ES, Neuberg D, Brown JR, Getz G and Wu CJ. Evolution and impact of subclonal mutations in chronic lymphocytic leukemia. Cell 2013; 152: 714-726.
[53] Zhang L, Chen J, Yang H, Pan C, Li H, Luo Y and Cheng T. Multiple microarray analyses identify key genes associated with the development of non-small cell lung cancer from chronic obstructive pulmonary disease. J Cancer 2021; 12: 996-1010.
[54] Duncan CJ, Mohamad SM, Young DF, Skelton AJ, Leahy TR, Munday DC, Butler KM, Morfopoulou S, Brown JR, Hubank M, Connell J, Gavin PJ, McMahon C, Dempsey E, Lynch NE, Jacques TS, Valappil M, Cant AJ, Breuer J, Engelhardt KR, Randall RE and Hambleton S. Human IFNAR2 deficiency: lessons for antiviral immunity. Sci Transl Med 2015; 7: 307ra154.
[55] Tanaka S, Hattori N, Ishikawa N, Horimasu Y, Deguchi N, Takano A, Tomoda Y, Yoshioka K, Fujitaka K, Arihiro K, Okada M, Yokoyama A and Kohno N. Interferon (alpha, beta and omega) receptor 2 is a prognostic biomarker for lung cancer. Pathobiology 2012; 79: 24-33.
[56] Remark R, Becker C, Gomez JE, Damotte D, Dieu-Nosjean MC, Sautès-Fridman C, Fridman WH, Powell CA, Altorki NK, Merad M and Gnjatic S. The non-small cell lung cancer immune contexture. A major determinant of tumor characteristics and patient outcome. Am J Respir Crit Care Med 2015; 191: 377-390.
[57] Fridman WH, Pagès F, Sautès-Fridman C and Galon J. The immune contexture in human tumours: impact on clinical outcome. Nat Rev Cancer 2012; 12: 298-306.
[58] Bruni D, Angell HK and Galon J. The immune contexture and immunoscore in cancer prognosis and therapeutic efficacy. Nat Rev Cancer 2020; 20: 662-680.
[59] Gobert M, Treilleux I, Bendriss-Vermare N, Bachelot T, Goddard-Leon S, Arfi V, Biota C, Doffin AC, Durand I, Olive D, Perez S, Pasqual N, Faure C, Ray-Coquard I, Puisieux A, Caux C, Blay JY and Ménétrier-Caux C. Regulatory T cells recruited through CCL22/CCR4 are selectively activated in lymphoid infiltrates surrounding primary breast tumors and lead to an adverse clinical outcome. Cancer Res 2009; 69: 2000-2009.
[60] Pan Y, Yu Y, Wang X and Zhang T. Tumor-associated macrophages in tumor immunity. Front Immunol 2020; 11: 583084.
[61] Dhodapkar KM, Gettinger SN, Das R, Zebroski H and Dhodapkar MV. SOX2-specific adaptive immunity and response to immunotherapy in non-small cell lung cancer. Oncoimmunology 2013; 2: e25205.
[62] Snyder AG, Hubbard NW, Messmer MN, Kofman SB, Hagan CE, Orozco SL, Chiang K, Daniels BP, Baker D and Oberst A. Intratumoral activation of the necroptotic pathway components RIPK1 and RIPK3 potentiates antitumor immunity. Sci Immunol 2019; 4: eaaw2004.

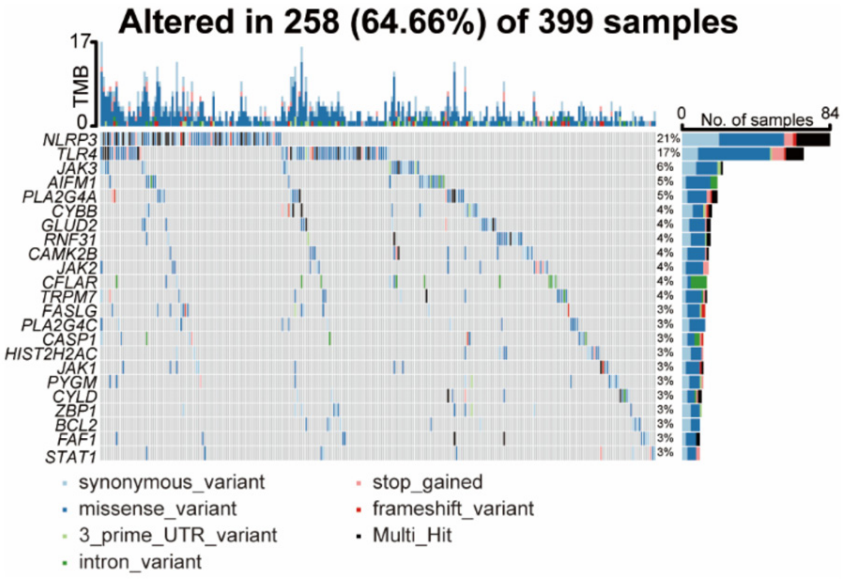

Supplementary Figure 1. The mutation landscape of NRGs in the TCGA-LUAD cohort. The mutation landscape of NRGs with a mutation rate of >3% in 399 LUAD patients from the TCGA-LUAD cohort. The waterfall plot showed the mutation information of each NRG with a mutation rate greater than 3%. The comments at the bottom of the corresponding hues indicated various types of mutations. The bar chart above described the tumor mutation burden (TMB). The bar chart and values on the right represented the mutation frequency of each NRG.

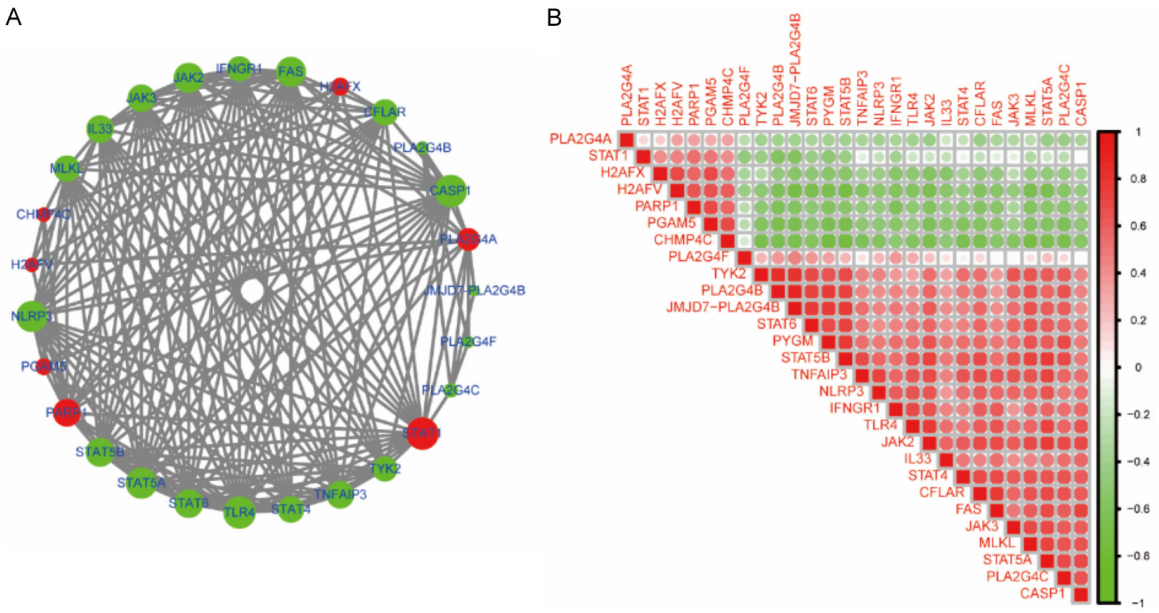

Supplementary Figure 2. Interaction network of the necroptosis-related DEGs. A. The protein-protein interaction (PPI) network of 28 necroptosis-related DEGs. The size of the node represents the multiple gene expression differences; up-regulated, red; down-regulated, green. B. The correlation heatmap of 28 necroptosis-related DEGs. Red represented positive correlation and green represented negative correlation.

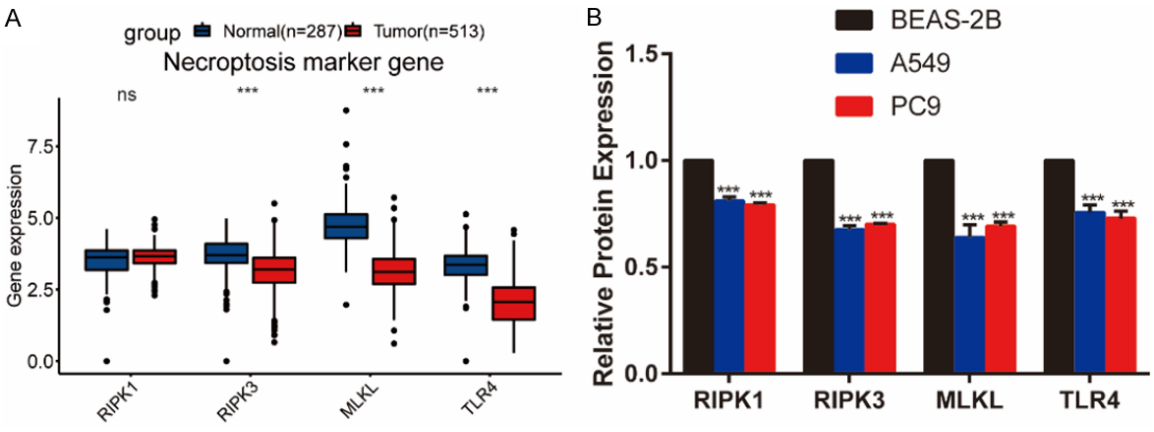

Supplementary Figure 3. The expression levels of necroptosis markers. A. The mRNA expression levels of necroptosis markers of LUAD and normal tissues in TCGA TARGET GTEx dataset. B. The relative protein expression levels of necroptosis markers in western blot. ns: no significance, ***P<0.001.

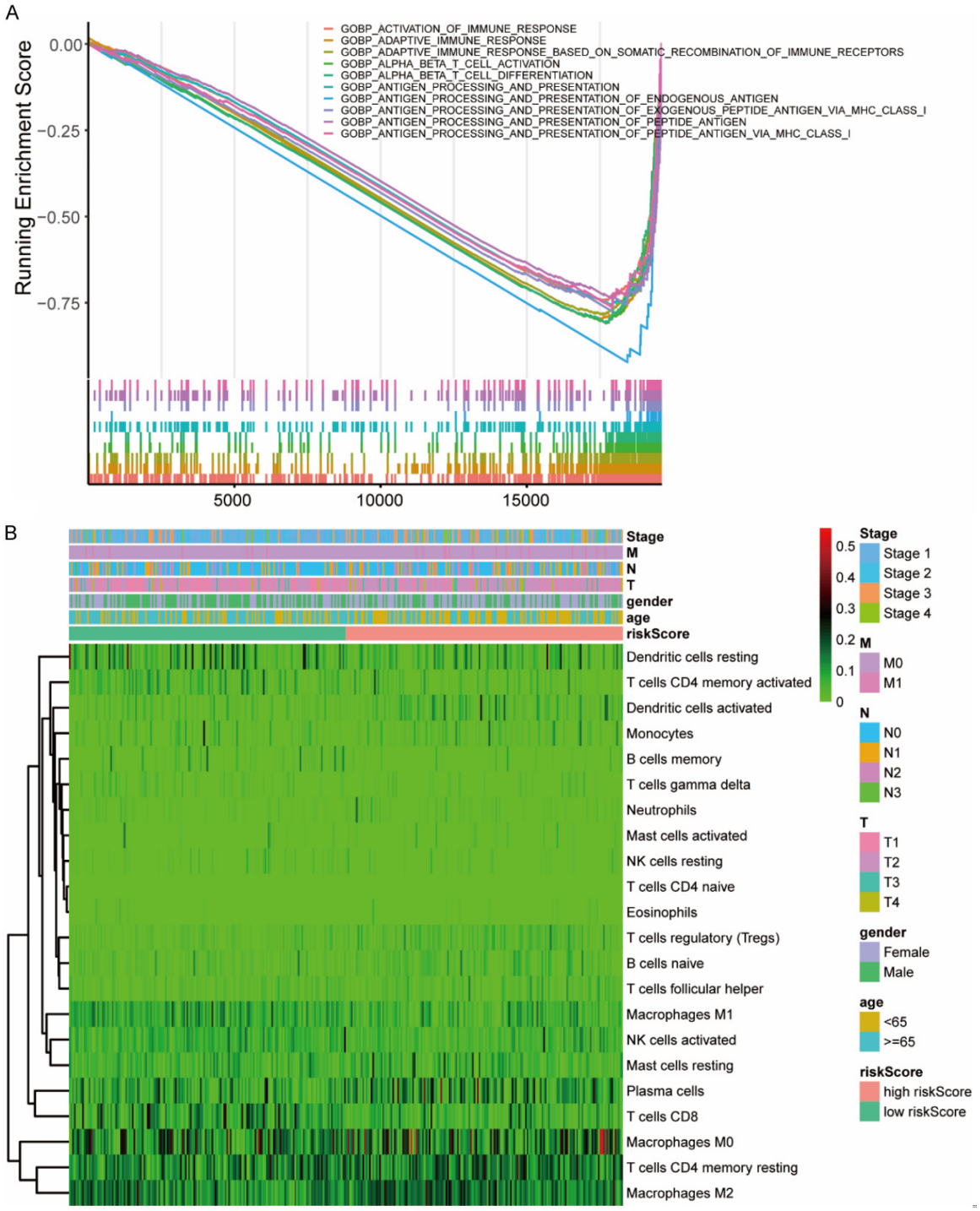

Supplementary Figure 4. Immunological characteristics between two risk score subgroups. A. Gene Set Enrichment Analysis (GSEA) between two risk score subgroups in the MSigDB collection (c5.all.v7.4.symbols.gmt). B. The 22 immune cells infiltration heatmap in the high-risk and low-risk score groups of the TCGA-LUAD cohort.

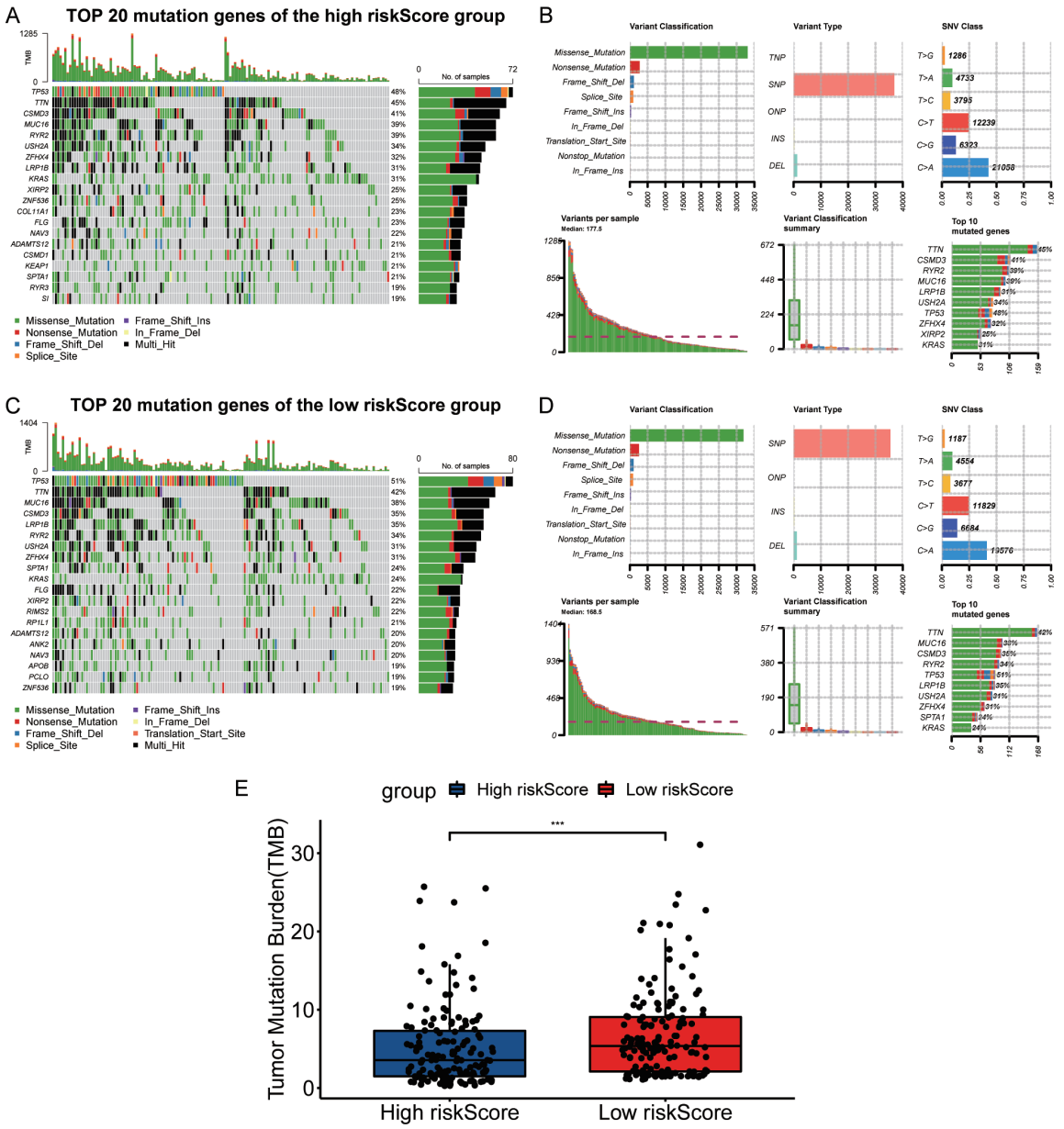

Supplementary Figure 5. Comparison of somatic mutation between two groups. A, B. The mutation frequency and classification of the high-risk score group. C, D. The mutation frequency and classification of the low-risk score group. E. Comparison of tumor mutation burden (TMB) between the two groups. ***P<0.001.

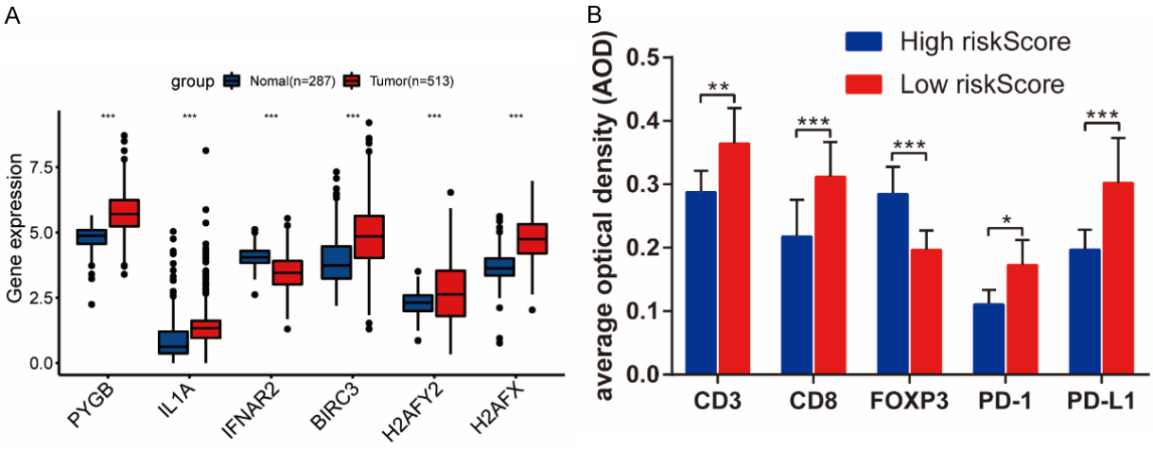

Supplementary Figure 6. Plots of statistical data for RT-qPCR and IHC analysis. A. Comparison of the expression levels of 6 necroptosis-related prognostic genes between LUAD and normal lung tissues in the TCGA TARGET GTEx dataset. B. Comparison of the average optical density (AOD) of immune cell markers and immune checkpoints between the two groups by IHC. ***P<0.001.